Applied Energy 334 (2023) 120653

Contents lists available at ScienceDirect

Applied Energy

journal homepage: www.elsevier.com/locate/apenergy

Future vehicle energy supply - sustainable design and operation of hybrid hydrogen and electric microgrids

Robert Förster [a,b,*], Matthias Kaiser [a,b], Simon Wenninger [a,b]

[a] Branch Business & Information Systems Engineering of the Fraunhofer FIT, Alter Postweg, 101, 86159 Augsburg, Germany
[b] FIM Research Center, University of Applied Sciences Augsburg, An der Hochschule, 1, 86161 Augsburg, Germany

HIGHLIGHTS

- Modelling hybrid charging and hydrogen refuelling microgrids.
- Optimisation of hybrid electric, hydrogen storage and stationary hydrogen fuel cell.
- Development of an optimisation model and application in a German case study.
- Cost-effective microgrid design and operation do not contribute to decarbonisation.
- Current demand charge regulation hinders profitability and low GHG operation.

GRAPHICAL ABSTRACT

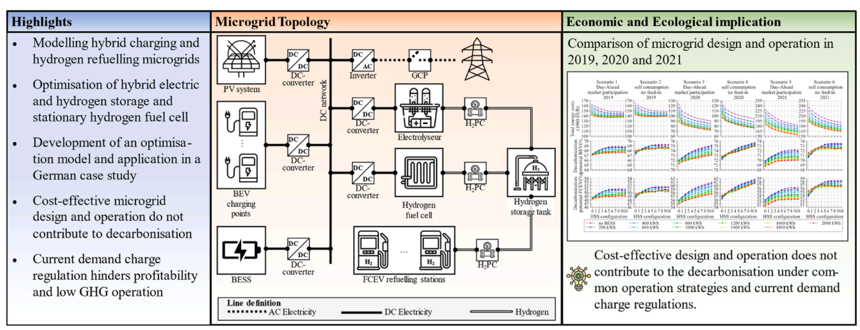

ARTICLE INFO

Keywords:
Microgrid
Hydrogen infrastructure
Electric vehicle charging
Hybrid energy storage systems
Decarbonization
Road transportation

ABSTRACT

To decarbonise road transport, EU policymakers promote battery electric vehicle and fuel cell electric vehicle adaption and advocate the expansion of charging and hydrogen refuelling infrastructure in the Fit-for-55 package. However, infrastructure operators face cost-intensive operations and insufficient low greenhouse gas (GHG) hydrogen availability. Grid-connected hybrid hydrogen refuelling and electric vehicle charging microgrids with on-site hydrogen production, battery and hydrogen energy storages and renewable energy can help to solve these challenges. We investigate the influence of various microgrid design and operation strategies regarding their contribution to profitability and decarbonisation in an optimisation study. Our findings in a real-world case study within Germany indicate that the cost-effectiveness of designing and operating such microgrids does not contribute to the decarbonisation of road transportation under common operation strategies and current demand charge regulations. We advocate revising German demand charge regulations to support sustainable design and operation of future charging and hydrogen refuelling microgrids.

1. Introduction

To mitigate the negative impacts of climate change and preserve the quality of life, it is necessary to comply with the Paris Agreement and preferably limit global warming to less than 1.5C compared to pre-industrial levels [1]. The “Fit for 55” package - developed by policymakers in the EU – aims to reduce Greenhouse Gas (GHG) emissions by 55 % until 2030 compared to 1990 levels [2]. Accounting for 23 % of energy-related GHG emissions, the decarbonisation of the transportation

* Corresponding author at: Branch Business & Information Systems Engineering of the Fraunhofer FIT, Alter Postweg, 101, 86159 Augsburg, Germany.
E-mail address: robert.foerster@fim-rc.de (R. Förster).

https://doi.org/10.1016/j.apenergy.2023.120653
Received 29 November 2022; Received in revised form 3 January 2023; Accepted 5 January 2023

Nomenclature

Sets and indices

t Index of time from $0, \cdots, T$
p Index of power plant types from $1, \cdots, P$

General parameters

m Length of time interval $[h]$

Parameters related to the Electrolyser (EL)

P^{EL} Relative energy consumption $[kWh/Nm^3]$
V^{EL}_{min} Minimal production capacity $[Nm^3/h]$
V^{EL}_{max} Maximal production capacity $[Nm^3/h]$

Parameters related to the Fuel Cell (FC)

V^{FC} Relative hydrogen demand $[Nm^3/kWh]$
P^{FC}_{min} Minimum electricity output $[kW]$
P^{FC}_{max} Maximal electricity output $[kW]$

Parameters related to the Hydrogen Storage Tank (HST)

V^{HST}_{min} Minimum volume of the HST $[Nm^3]$
V^{HST}_{max} Maximum volume of the HST $[Nm^3]$
V^{HST}_{ini} Initial hydrogen filling level $[Nm^3]$

Parameters related to the Battery Energy Storage System (BESS)

E^{BESS}_{cap} Rated energy capacity $[kWh]$
SOC^{BESS}_{min} Minimal acceptable State of Charge (SoC)[%]
SOC^{BESS}_{max} Maximum acceptable SoC [%]
SOC^{BESS}_{ini} Initial SoC [%]
P^{BESS}_{rated} Rated charging and discharging power $[kW]$
$SOC^{BESS,tap}_{ch}$ Tapering parameter limiting charging power at high SoC [%]
$SOC^{BESS,tap}_{dis}$ Tapering parameter limiting discharging power at low SoC [%]
η^{BESS}_{ch} Charging efficiency [%]
η^{BESS}_{dis} Discharging efficiency [%]

External parameters

P^{GCP}_{max} Maximum possible power flow at Grid Coupling Point (GCP)$[kW]$
EP^{in} Retail price for electricity drawn from the grid $[EUR/kWh]$
EP^{out} Grid feed-in price for electricity $[EUR/kWh]$
EP^{dcr} Demand charge rate imposed by the grid operator $[EUR/kW$ per year$]$
$P^{BEV,d}_t$ Charging demand of Battery Electric Vehicles (BEV) in period $t[kW]$
$V^{FCEV,d}_t$ Hydrogen demand of Fuel Cell Electric Vehicles (FCEV) in period $t[Nm^3]$

Variables related to the BESS

y^{BESS}_t Binary variable with $y^{ESS}_t = 1$, when BESS is charged in period t, else $y^{ESS}_t = 0$.
SOC^{BESS}_t SoC of the BESS in period t[%]
$P^{BESS,ch}_t$ Charging power of the BESS in period $t[kW]$
$P^{BESS,dis}_t$ Discharging power of the BESS in period $t[kW]$

Variables related to the Hydrogen Subsystem (HSS)

y^{EL}_t Binary variable with $y^{EL}_t = 1$, when electrolysis is carried out in period t, else $y^{EL}_t = 0$
$P^{EL,d}_t$ Power demand of the EL in period $t[kW]$
$V^{EL,prod}_t$ Hydrogen production volume in period $t[Nm^3]$
V^{HST}_t Stored hydrogen volume at the End of period t $[Nm^3]$
y^{FC}_t Binary variable with $y^{FC}_t = 1$, when FC generates power in period t, else $y^{FC}_t = 0$.
$P^{FC,out}_t$ Power output of the FC in period $t[kW]$
$V^{FC,d}_t$ Hydrogen demand of the FC in period $t[Nm^3]$
$V^{HST,FCEV}_t$ Hydrogen supplied to the FCEV in period $t[Nm^3]$
$V^{HST,FC}_t$ Hydrogen supplied to the FC in period $t[Nm^3]$

Variables related to the power demand and supply

P^{MG}_t Total power in the microgrid in period $t[kW]$
$P^{grid,in}_t$ Power drawn from the public power grid in period $t[kW]$
$P^{grid,out}_t$ Power fed into the public power grid in period $t[kW]$
y^{grid}_t Binary variable with $y^{grid}_t = 1$, when electricity is drawn from the power grid in period t, else $y^{grid}_t = 0$.
P^{grid}_{max} Peak load at the GCP $[kW]$
$P^{BEV,ch}_t$ Power used for charging BEV in period $t[kW]$

Variables and Parameters related to the Photovoltaic (PV) system

P^{PV}_t Power output of the PV system in period $t[kW]$
N^{PV} Number of installed PV modules
$P^{PV,STC}$ Power output of one PV module under Standard Test Conditions (STC)$[kW]$
GHI_t Global horizontal irradiance in period $t[W/m^2]$
GHI^{STC} Global horizontal irradiance used for STC $[W/m^2]$
GHI^{NOCT} Global horizontal irradiance at Nominal Operating Cell Temperature $[W/m^2]$
γ Temperature coefficient for power at the maximum power point $[\%/^{\circ}C]$
T^C_t Cell temperature in period t[°C]
$T^{C,STC}$ Cell temperature under STC [°C]
T^{amb}_t Ambient temperature in period t
T^{NOCT} Cell temperature at NOCT [°C]
$T^{amb,NOCT}$ Ambient temperature at NOCT [°C]

Variables and Parameters related to the decarbonisation evaluation

$\bar{e}^{grid}_t$ Emission factor for grid electricity in period $t[gCO_2-eq/kWh]$
$\bar{e}^{MG}$ Average microgrid emission factor $[gCO_2-eq/kWh]$
$P^{feed-in}_{p,t}$ Feed-in power of power plants of type p in period $t[MW]$
e_p Emission factor for power plant type $p[gCO_2-eq/kWh]$
dcp^{BEV} Decarbonisation potential of BEV [%]
dcp^{FCEV} Decarbonisation potential of FCEV [%]
$E^{BEV,ch}$ BEV energy consumption $[kWh/100km]$
$V^{FCEV,rf}$ FCEV hydrogen consumption $[Nm^3/100km]$
$e^{ICE,car}$ Emission factor of one passenger car with an Internal Combustion Engine (ICE)$[gCO_2-eq/100km]$
$e^{ICE,truck}$ Emission factor of one heavy-duty truck with ICE $[gCO_2-eq/100km]$

sector holds significant potential to archive the GHG reduction targets [3]. Researchers predict that Battery Electric Vehicles (BEV) for short-distance individual transport and Fuel Cell Electric Vehicles (FCEV) for heavy-duty long-distance transport will share a coexistence in decarbonised road transportation [4–7]. Besides decarbonisation, the promotion and long-term deployment of electrified and hydrogen-based technologies in the transportation sector is also designed to reduce the EU dependency on fossil fuels from Russia as part of the REPowerEU plan following the start of the Russian-Ukrainian war [8]. For a significant market uptake, publicly accessible and comprehensive charging and hydrogen refuelling infrastructure are required [9–11], which are not widely deployed in Europe yet [12]. Therefore, the "Fit for 55" package includes requirements for a cross-European network of charging and hydrogen refuelling stations. This implies that by 2030, EU Member States have to install a charging option for BEVs every 60 km and a refuelling option for FCEVs every 100 km along the trans-European transportation network (i.e., important national motorways) [2,13,14].

Following this legislative proposal, massive investments in infrastructure projects in the current decade are necessary, which the private sector is reluctant to make in present market conditions [15–17]. Policymakers have recognised the urgent need for action and have already launched initial initiatives and strategies [18,19]. For example, national hydrogen strategies attempt to comply with the legislative proposal by providing investment incentives [20]. However, several challenges hinder further expansion of microgrid projects for decarbonised road transportation. First, practitioners face cost-intensive operation [21,22]. Second, there is no distribution network to transfer hydrogen across long distances available in the EU yet [23]. Third, to realise the long-term vision of carbon neutrality, the electricity for charging BEVs and producing hydrogen via electrolysis needs to be generated from Renewable Energy Sources (RES) [24], making demand-side management measures and energy storage necessary, to address the volatility of RES supply [25,26].

Thus, for future charging and hydrogen refuelling stations, decentralised generation of renewable energy, on-site hydrogen production and ability to store energy might be crucial. Microgrids - small, decentralised electricity distribution grids - connecting renewable generation, energy storage and hydrogen production technologies to provide charging and hydrogen refuelling possibilities, promise to address and solve the presented challenges. As a solution, a grid-connected microgrid that uses electricity from RES for charging stations along with hydrogen generation and a hybrid battery-hydrogen energy storage system can be feasible [27,28]. Decentral hydrogen generation can meet the surging demand with no hydrogen distribution grids established yet and no clarity on national generation or import. In practice, Battery Energy Storage Systems (BESS) help to compensate short-term fluctuations in local energy supply [29], while hydrogen is rather used as a long-term energy storage medium, due to its higher energy density compared to batteries [30].

However, previous studies consider only partial aspects of microgrid design and operational strategies to synergistically serve both BEVs and FCEVs and incorporate both energy storage options. Decision-makers still lack techno-economic guidance for designing and operating the outlined hybrid charging and hydrogen refuelling station microgrid with low GHG emissions. To ensure profitable, low GHG, and seamless operation, it is necessary to study the design and operation strategy of the installed units in the microgrid in detail. We intend to fill this gap in research and pave the way for widespread application in the future charging and hydrogen refuelling infrastructure for decarbonised road transportation. We present a microgrid and introduce a mathematical optimisation model that aims for minimising total energy cost during operation of the outlined microgrid. Using data from a real-world case study in Germany, we investigate the influence of Electrolyser (EL) and Fuel Cell (FC) power as well as capacities of a hybrid hydrogen and battery energy storage system on operation, total energy costs and the decarbonisation potential of BEV and FCEV. Optimising different operational strategies of Day-Ahead market participation and self-consumption in 2019, 2020 and 2021 allows us to derive the effects of component sizing and grid demand charges under diverse conditions. We contribute to the development of technical, economic, and design guidelines to support investors and operators in the development of future hybrid charging and hydrogen refuelling stations and the transformation of fossil fuel-based gas stations. Further, this paper contributes to policy measures as our results shed light on existing regulatory barriers to low GHG operation of future charging and hydrogen microgrids in mobility.

2. The microgrid paradigm and related literature

Due to cross-sector decarbonisation and electrification, microgrids are becoming increasingly popular to address the challenge of volatile power supply from renewable energy sources and the diversity of new electricity consumers. According to Ton and Smith [31] and Hirsch et al. [32] we define microgrids as follows: The term microgrid refers to energy distribution networks that may operate connected to or disconnected from a larger macrogrid, commonly the public electricity grid. Grid-connected microgrids usually have one Grid Coupling Point (GCP), from which electricity can be drawn or also fed into the grid. Most researchers agree that a grid-connected microgrid should be able to operate in both grid and island mode and perform a seamless transition. In this paper, we adopt the concept of temporary off-grid operation, as it is the most realistic scenario for a future widespread charging and hydrogen refuelling infrastructure in Germany and the EU, along with being economically viable for prosumer infrastructures [33].

Researchers focus on different microgrid characteristics depending on the specific application, including grid-connectivity, RES integration, use of BESS and hydrogen production to serve load demands such as BEV-charging and FCEV-refuelling. The literature in this field (cf. Table 1) reveals different research objectives as Design principles and operation strategies. When it comes to any RES-based microgrid system, a key consideration is the sizing of the power generation capacity [34–36]. Mah et al. [34] analyse the sizing of RES regarding the profitability for operators in islanded microgrid settings. As Li et al. [37] stated, the operating strategy has a significant impact on the economic design of individual units in the microgrid. To improve the self-sufficiency and profitability of RES-integrated microgrids, Bahramirad et al. [38] investigate the integration of BESS that contribute to higher decarbonisation potential. Several economic barriers hinder the widespread expansion of charging infrastructure, including high annual demand charge rates due to peak charging demand [39]. Xiang et al. [40] investigate the design of an airport microgrid focusing on charging BEVs and meeting electric loads of aircraft through RES and confirm the viability of BESS in reducing power peaks.

As BESSs are expensive and therefore a major factor in investment decisions [41,42], Haupt et al. [29] focus on the sizing of BESSs for a renewable fast charging hub microgrid, considering different charging strategies and real-world data-driven demand forecasts. To further exploit the benefits of RES, a hydrogen energy storage system can be applied in microgrids with BESS [43]. While BESS are used to cover short-term demand and supply fluctuations, hydrogen as energy storage is mainly used for long term energy management in microgrids [44]. Addressing different application areas with hydrogen loads or long-term microgrid self-sufficiency, microgrid designs are proposed which include hydrogen production and storage [36,45–50]. In their research, Baghaee et al. [46] demonstrate long-term energy management based on hydrogen in remote, islanded microgrids. Yamashita et al. [51] investigate microgrids in residential and public buildings, focusing on operating strategies for hybrid hydrogen and battery energy storage systems to maintain supply reliability and increase self-sufficiency. The inclusion of hydrogen generation and reconversion can improve the autonomy of microgrids if all related components are scaled

Table 1
Literature review on microgrid research categorised by microgrid characteristics, application, and research focus.

Reference	Microgrid characteristic						Application		Research focus	
	Grid-connected Microgrid	Volatile RES feed-in	Stationary BESS	Hydrogen production via EL	Hydrogen reconversion via FC	Stationary hydrogen storage	EV charging	Hydrogen refuelling	Design guidelines	Operational strategies
Alam et al. [43]		✓			✓	✓			✓	✓
Alavi et al. [45]	✓	✓		✓	✓	✓		✓	✓	
Aslani et al. [52]		✓		✓	✓	✓	✓	✓		✓
Baghaee et al. [46]		✓		✓	✓	✓			✓	
Bahramirad et al. [38]	✓	✓	✓						✓	
Coppitters et al. [49]	✓	✓	✓	✓	✓	✓			✓	✓
Dawood et al. [58]		✓	✓	✓	✓	✓			✓	
Ding et al. [41]	✓		✓				✓		✓	
Dispenza et al. [59]	✓	✓	✓	✓		✓	✓	✓	✓	
Grüger et al. [54]	✓	✓		✓		✓		✓	✓	
Han et al. [57]		✓	✓	✓	✓	✓			✓	✓
Han et al. [56]		✓	✓	✓	✓	✓	✓		✓	✓
Haupt et al. [29]	✓	✓	✓				✓		✓	
Jacob et al. [35]		✓	✓	✓	✓	✓			✓	
Khiareddine et al. [42]		✓	✓	✓	✓	✓			✓	
Kyriakarakos et al. [53]		✓	✓	✓	✓	✓		✓	✓	
Li et al. [37]		✓	✓	✓	✓	✓			✓	✓
Liu et al. [60]	✓	✓	✓	✓	✓	✓	✓	✓	✓	✓
Mah et al. [34]		✓	✓	✓	✓	✓			✓	✓
Mansour-Saatloo et al. [27]	✓	✓	✓	✓	✓	✓	✓	✓		✓
Tobajas et al. [50]	✓	✓	✓	✓	✓	✓				✓
Vafaei and Kazerani [47]		✓		✓	✓	✓			✓	
Valverde et al. [44]		✓	✓	✓	✓	✓			✓	✓
Vivas et al. [61]	✓	✓	✓	✓	✓	✓				✓
Xiang et al. [40]	✓	✓	✓	✓	✓	✓	✓		✓	
Xu et al. [48]		✓		✓	✓	✓	✓	✓		✓
Xu et al. [55]	✓	✓		✓	✓	✓	✓			✓
Yamashita et al. [51]	✓	✓	✓	✓	✓	✓				✓
Zhang et al. [62]		✓	✓	✓	✓	✓	✓	✓		✓
Zhao and Brouwer [36]		✓		✓	✓	✓		✓	✓	✓

appropriately [52]. Yet, both design and operation complexity is significantly higher [53].

In addition, the design of hydrogen refuelling stations with decentralised hydrogen production should consider the demand behaviour [54] and availability of RES [55]. Alavi et al. [45], investigate synergies between demand in refuelling FCEVs and reconversion through FC in FCEV in residential microgrids to achieve higher self-sufficiency of hydrogen refuelling stations. While Han et al. [56] and Han et al [57] focused on the operation of islanded hybrid hydrogen-battery microgrids in consecutive studies, Dawood et al. [58] compared scenarios using BESS only, hydrogen energy storage only and hybrid battery-hydrogen energy storage regarding investment costs, operational costs and GHG reduction potential. Dispenza et al. [59] investigate a solar-powered mobility hub including charging and hydrogen refuelling infrastructure for public transport. In the absence of a BESS, Xu et al. [48] focus on operational strategies of reconverted excess hydrogen via stationary FC to serve the stochastic demand of BEV in a RES based standalone microgrid for recharging BEV and refuelling FCEV to promote the market uptake of these propulsion technologies. Mansour-Saatloo et al. [27] propose operational strategies for microgrids incorporating hydrogen, heat and electric loads microgrid, including both BEV and FCEV demand. Their research analyses cost reduction potential through different design variations, with BESS resulting in a slighter impact on total cost reduction than implementing a hydrogen energy storage system. In the combined scenario with a hybrid battery and hydrogen energy storage system, a reduction in operating costs of more than three quarters can be measured. Similarly, Liu et al. [60] investigate operational strategies to organise charging and hydrogen refuelling in a case study for residential high-rise buildings, considering different cruise schedules and, therefore, different demands for BEV-charging and FCEV-refuelling. Their analysis of different energy management strategies reveals that hydrogen is less prioritised as an energy storage medium if battery capacity is high.

As reflected, multiple microgrid approaches with varying characteristics can be identified in the literature, focusing on partial aspects of design principles and operational strategies to address objectives such as high self-sufficiency. Various highlighted research articles provide an outlook on synergies between the charging of BEVs and the operation of hydrogen refuelling stations with integrated hydrogen production [27,48,59,60]. So far, previous research has neglected to investigate future BEV/FCEV supply on highway corridors through microgrids which include charging and hydrogen refuelling infrastructure with a focus on component sizing and operating strategies to reduce total energy costs and GHG emissions.

3. Research design

3.1. Microgrid topology design

Our study investigates a microgrid that provides high-performance hybrid charging and hydrogen refuelling services. We, therefore, design a grid-connected microgrid with BEV charging points, FCEV refuelling stations, an on-site Photovoltaic (PV) system, EL, FC, BESS and HST, as illustrated in Fig. 1.

We consider electrical energy flows and volumetric hydrogen flows within this microgrid setting. Electrical power can be converted from the local PV System or drawn from the power grid via the GCP. Microgrids generally share the advantage of low electrical losses during voltage conversion and distribution if the renewables are located close to the consuming units [63]. Therefore, an on-site PV array system is used as the on-site source of electricity from RES. We further propose a Direct Current (DC) system to reduce conversion losses and increase overall efficiency as recommended in multiple publications [64–68]. As all supply and load technologies in the microgrid use DC, we only need one Alternating Current (AC) to DC converter at the GCP. The more efficient DC to DC converters between the DC technologies ensure the operation of differently required power levels within the network. Hydrogen electrolysis technologies are categorised into alkaline electrolysis, solid oxide electrolysis and proton exchange membrane (PEM) electrolysis. In our study, we focus on PEM electrolysers as they feature high efficiency, high operational flexibility and yield high hydrogen purity for prospective applications in fuel cells such as FCEV and stationary auxiliary electricity generation [69]. We use electricity-powered PEM electrolysis of water for hydrogen production [70] to either directly satisfy hydrogen loads or to store in a stationary HST in gaseous form [71]. Total emissions from electrolysis can be controlled by the electricity mix used [72], causing high GHG emissions with fossil fuels and low GHG emissions with RES [20]. In addition to hydrogen storage, a BESS is deployed to store electrical energy. We consider lithium-ion batteries for the BESS because of their high energy density and low standby self-discharge

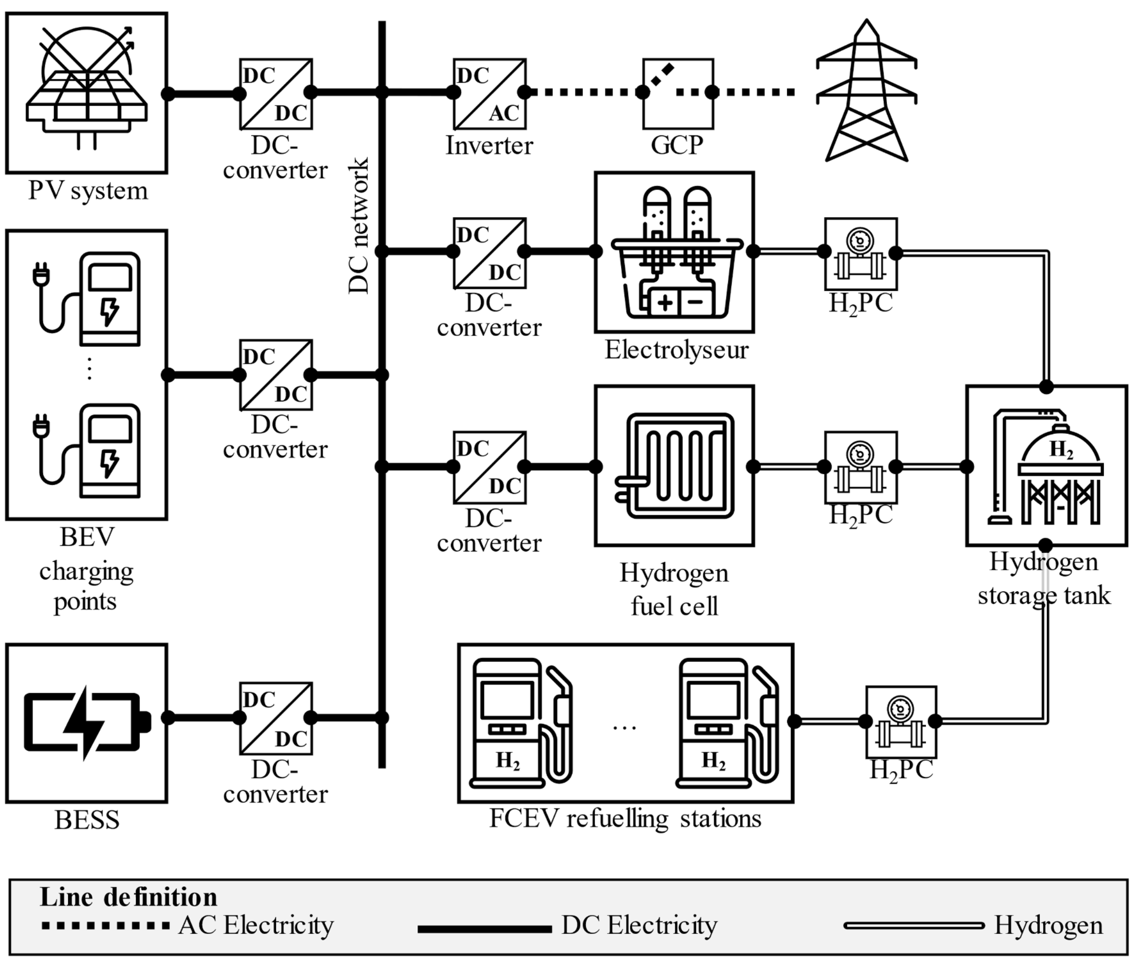

Fig. 1. Illustration of the microgrid and its system modules.

[73]. Hydrogen can also be reconverted into electricity by a FC. FCs are categorised into alkaline FCs, phosphoric acid FCs, proton exchange membrane fuel cells (PEMFCs), molten carbonate FCs and solid oxide FCs [74]. This study considers PEMFC technology to reconvert hydrogen, allowing high efficiency with fast ramp-up times, reliable and flexible operation and high power density [75,76]. For both EL and FC, the ability of fast ramp-up and flexible operation enable the coverage of volatile mobility energy demand for electricity and hydrogen. The EL, HST and FC collectively form the hydrogen subsystem (HSS). The hydrogen produced by the EL must be compressed to the required pressure to be stored in the HST or to be provided to the FCEV refuelling stations. Also, pressurized hydrogen must be expanded before it can be converted to electricity in the FC. The ambient temperature affects the pressure of the stored hydrogen and can pose a potential safety risk, thus pressure must be controlled adequately. By applying hydrogen pressure controller (H_2PC), we consider both mechanical compressors and pressure regulating valves in the HSS. The charging and hydrogen refuelling services at the EV charging points, and FCEV refuelling stations are the main electricity and hydrogen consumers.

3.2. Modelling microgrid operation

The illustrated microgrid in Fig. 1 represents a diverse and integrated system including the subsystems, such as the PV system or the BEV charging points, which generally can operate autonomously. However, within the microgrid the subsystems are controlled towards a shared objective. The capability of the subsystems to exchange information, to execute and assign tasks and to pursue collective objectives is characteristic for a so called system of systems [77–79]. For the operation of such microgrids, a dedicated energy management system or microgrid control system is applied to determine and control the ideal operating state [80]. Several optimisation techniques are available for microgrids ranging from iterative and graphical optimisations to artificial intelligence driven methods [81]. To achieve the overall objective of the microgrid, we employ a mixed integer linear programming model (MILP) to optimise the operation of the microgrid, as established for similar problems in research [29,34,42,46,49]. As in common practice for the microgrid system of systems [79], we organise the subsequent model formulation upon the various subsystems and the shared microgrid objective.

The optimisation aims to minimise the total energy cost by scheduling the use of BESS, EL, FC and HST and is limited by several constraints (cf. equation (1)). The objective function includes three components. First, the annual grid demand charges corresponding to the peak demand P^{grid}_{max} and the linear demand charge rate EP^{dcr}, second, the volume-based electricity procurement costs for the power drawn from the public grid $P^{grid,in}_t$ multiplied with the electricity price EP^{in}_t and third, the revenues for the electricity fed into the grid $P^{grid,out}_t$ compensated with the feed-in price EP^{out}_t for all periods t. The factor m allows to consider different time intervals and thereby ensures consistency in the respective units.

$$\min C:\ P^{grid}_{\max}\cdot EP^{dcr}+\sum_{t=0}^{T}\left[\left(P^{grid,in}_t\cdot EP^{in}_t-P^{grid,out}_t\cdot EP^{out}_t\right)\cdot m\right] \quad (1)$$

Here, P^{grid}_{max} is the load peak at the GCP over the total time frame under examination (cf. equation (2)).

$$P^{grid}_{max}=max\left\{P^{grid,in}_t,P^{grid,out}_t\right\} \quad \forall t\in T \quad (2)$$

Although electricity can be drawn from the power grid, the preferred electricity source is the on-site PV system. The power output of the PV system P^{PV}_t in each period $t\in T$ (cf. equation (3)) depends on the number of installed PV modules N^{PV}, the power output of one PV module under Standard Test Conditions (STC) $P^{PV,STC}$, the irradiance GHI_t, the irradiance used in STC GHI^{STC}, the temperature coefficient for power at the maximum power point γ, the cell temperature T^C_t and the cell temperature under STC $T^{C,STC}$. The T^C_t depends on the ambient temperature T^{amb}_t, the irradiance GHI_t, the irradiance at Normal Operating Cell Temperature (NOCT) GHI^{NOCT}, the cell temperature at NOCT T^{NOCT} and the ambient temperature at NOCT $T^{amb,NOCT}$ as stated in equation (4) [82–84].

$$P^{PV}_t=N^{PV}\cdot P^{PV,STC}\cdot\frac{GHI_t}{GHI^{STC}}\cdot\left[1-\gamma\cdot\left(T^C_t-T^{C,STC}\right)\right] \quad \forall t\in T \quad (3)$$

$$T^C_t=T^{amb}_t+\frac{GHI_t}{GHI^{NOCT}}\cdot\left(T^{NOCT}-T^{amb,NOCT}\right) \quad \forall t\in T \quad (4)$$

The operation of the BESS, EL, FC and HST within the microgrid is subject to several constraints. As introduced in Section 3.1, there are several types of electricity supply units and electricity consumption units in the microgrid. Equations (5) and (6) state that the power balance, i.e., the balance between electricity supply, i.e., grid purchase $P^{grid,in}_t$, on-site PV generation P^{PV}_t, BESS discharge $P^{BESS,dis}_t$, FC generation $P^{FC,out}_t$ and electricity demand, i.e., electricity feed-in $P^{grid,out}_t$, electric vehicle charging $P^{BEV,ch}_t$, BESS charging $P^{BESS,ch}_t$, EL power demand $P^{EL,d}_t$, must always be met.

$$P^{MG}_t=\left(P^{grid,in}_t+P^{PV}_t+P^{BESS,dis}_t+P^{FC,out}_t\right)-\left(P^{grid,out}_t+P^{BEV,ch}_t+P^{BESS,ch}_t+P^{EL,d}_t\right) \quad \forall t\in T \quad (5)$$

$$P^{MG}_t=0 \quad \forall t\in T \quad (6)$$

The maximum power that can be purchased from or fed into the public grid through the GCP P^{GCP}_{max} within a given period is limited by the rating of the inverter between the microgrid and the public grid. Thus, the amount of electricity drawn from the public grid must remain within a range defined by (7) and (8). These constraints also prevent simultaneous drawing and feeding in electricity. Therefore, the binary variable y^{grid}_t decides whether power can be drawn ($y^{grid}_t=1$) or fed into ($y^{grid}_t=0$) the public grid.

$$0\le P^{grid,in}_t\le P^{GCP}_{max}\cdot y^{grid}_t \quad \forall t\in T \quad (7)$$

$$0\le P^{grid,out}_t\le P^{GCP}_{max}\cdot\left(1-y^{grid}_t\right) \quad \forall t\in T \quad (8)$$

The BESS is dedicated to the storage of electrical energy in the microgrid and modelled according to 29 [29]. It is not possible to simultaneously charge and discharge the BESS. Constraints (9) and (10) ensure that the BESS can either be charged or discharged, as the binary variable $y^{BESS}_t=1$ reflects charging and $y^{BESS}_t=0$ reflects discharging the battery within the technically given power range limited by the rated charging and discharging power P^{BESS}_{rated}.

$$0\le P^{BESS,ch}_t\le P^{BESS}_{rated}\cdot y^{BESS}_t \quad \forall t\in T \quad (9)$$

$$0\le P^{BESS,dis}_t\le P^{BESS}_{rated}\cdot\left(1-y^{BESS}_t\right) \quad \forall t\in T \quad (10)$$

For any period, except for the initial period $t=0$, the State of Charge (SoC) of the BESS (SOC^{BESS}_t) is calculated by the SoC of the previous period plus the change in the SoC level through charging ($P_t^{BESS,ch}$) or discharging ($P_t^{BESS,dis}$), respective of the charging (η_{ch}^{BESS}) and discharging efficiency (η_{dis}^{BESS}), in relation to the BESS energy capacity E_{cap}^{BESS} (cf. equation (11)).

$$SOC_t^{BESS} = SOC_{t-1}^{BESS} + \frac{m\cdot\left(P_t^{BESS,ch}\cdot\eta_{ch}^{BESS} - P_t^{BESS,dis}/\eta_{dis}^{BESS}\right)}{E_{cap}^{BESS}} \quad \forall t > 0 \tag{11}$$

As the power consumption and power output performance of BESS Systems significantly decrease at low $\left(SOC_t^{BESS} < 20\%\right)$ and high $\left(SOC_t^{BESS} > 80\%\right)$ SoCs, charging and discharging processes slow down within these SoC ranges [85]. Therefore, it may be desirable to avoid low and high SoC, thus limiting the allowed range of operation between the minimal SoC $\left(SOC_{min}^{BESS}\right)$ and the maximal SoC $\left(SOC_{max}^{BESS}\right)$ as stated in constraint (12).

$$SOC_{min}^{BESS} \le SOC_t^{BESS} \le SOC_{max}^{BESS} \quad \forall t \in T \tag{12}$$

If BESS operation in low and high SoC ranges is applied, the rated charging $\left(P_t^{BESS,ch}\right)$ and discharging power $\left(P_t^{BESS,dis}\right)$ of the BESS must be limited [29]. In equation (13), the charging power is derated in high SoC ranges $\left(SOC_{ch}^{BESS,tap}\right)$, and in (14), the discharging power is derated in low SoC ranges $\left(SOC_{dis}^{BESS,tap}\right)$.

$$P_t^{BESS,ch} \le \frac{-1\cdot P_{rated}^{BESS}}{1 - SOC_{ch}^{BESS,tap}}\cdot\left(SOC_t^{BESS} - 1\right) \quad \forall t \in T \tag{13}$$

$$P_t^{BESS,dis} \le \frac{P_{rated}^{BESS}}{SOC_{dis}^{BESS,tap}}\cdot\left(SOC_t^{BESS}\right) \quad \forall t \in T \tag{14}$$

Optimisation models require predefined starting conditions. We specify an initial value $SOC_{ini}^{BESS,SoC}$ for the SoC of the BESS in period $t = 0$, which corresponds to the permissible range described in equation (12). This SoC level must recover in the last period T to avoid any distortion due to the used amount of energy.

$$SOC_0^{BESS} = SOC_T^{BESS} = SOC_{ini}^{BESS} \tag{15}$$

During EL operation, the binary decision variable sets to $y_t^{EL} = 1$ and hydrogen is produced within the permitted power range as stated in equation (17). The amount of produced hydrogen $V_t^{EL,prod}$ depends on the power $P_t^{EL,d}$ used to operate the EL. In (16), we assume a proportional relationship between the hydrogen output and electricity input of the EL P^{EL}. Since the efficiency of the EL decreases in low power ranges [86], this proportional relation does not hold for the entire operating range of the EL. Therefore, we limit the performance range between the minimal hourly hydrogen output V_{min}^{EL} and the maximal hourly hydrogen output V_{max}^{EL} as modelled in (17).

$$V_t^{EL,prod} = \frac{P_t^{EL,d}}{P^{EL}}\cdot m \quad \forall t \in T \tag{16}$$

$$V_{min}^{EL}\cdot y_t^{EL}\cdot m \le V_t^{EL,prod} \le V_{max}^{EL}\cdot y_t^{EL}\cdot m \quad \forall t \in T \tag{17}$$

Similar to the EL, we assume a proportional relationship between the hydrogen input $V_t^{FC,d}$ and electrical power output $P_t^{FC,out}$ of the FC, when the FC is in operation and the binary decision variable is set to $y_t^{FC} = 1$. (cf. equation (18)). Analogous to the electrolysis, we limit the operating power range of the FC, due to technical design constraints of the FC and varying efficiencies in low, below P_{min}^{FC}, and high power ranges, above P_{max}^{FC}, [87] (cf. equation (19)).

$$P_t^{FC,out} = \frac{V_t^{FC,d}}{V^{FC}\cdot m} \quad \forall t \in T \tag{18}$$

$$P_{min}^{FC}\cdot y_t^{FC} \le P_t^{FC,out} \le P_{max}^{FC}\cdot y_t^{FC} \quad \forall t \in T \tag{19}$$

Through the addition of a hydrogen storage tank, hydrogen production $V_t^{EL,prod}$ and consumption is time-decoupled, which gives the system increased flexibility. The storage level of the hydrogen storage tank V_t^{HST} at any period is defined by the level of the previous period and the current hydrogen inflows and outflows (20).

$$V_t^{HST} = V_{t-1}^{HST} + V_t^{EL,prod} - V_t^{HST,FCEV} - V_t^{FC,d} \quad \forall t > 0 \tag{20}$$

The size, the working pressure and the temperature limit the capacity of the HST. For operation, the level of the storage tank must be within the minimum $\left(V_{min}^{HST}\right)$ and maximum capacity $\left(V_{max}^{HST}\right)$, represented by equation (21). Similar to the BESS, an initial HST level V_{ini}^{HST} must be defined, which must be reached again in the last period T (cf. equation (22)).

$$V_{min}^{HST} \le V_t^{HST} \le V_{max}^{HST} \quad \forall t \in T \tag{21}$$

$$V_0^{HST} = V_T^{HST} = V_{ini}^{HST} \tag{22}$$

As we analyse the case of a charging and refuelling station near motorways, we assume customers primarily request immediate charging, thus we exclude controlled and bidirectional charging strategies. Accordingly, we assume that each BEV starts charging in the period it arrives at the station and ends charging as soon its demand is satisfied. Therefore, the provided charging power $P_t^{BEV,ch}$ must be equal to the aggregated BEV charging demand $P_t^{BEV,d}$ (cf. equation (23)). In addition, we assume that the number of charging points is sufficient to serve all arriving BEVs. Consistent with the chosen BEV charging strategy and the assumptions made, immediate FCEV refuelling is applied. Furthermore, the FCEV cannot be refuelled with more hydrogen than demanded $\left(V_t^{FCEV,d}\right)$ (cf. equation (24)).

$$P_t^{BEV,d} - P_t^{BEV,ch} = 0 \quad \forall t \in T \tag{23}$$

$$V_t^{FCEV,d} - V_t^{HST,FCEV} = 0 \quad \forall t \in T \tag{24}$$

3.3. Microgrid configuration and scenario analysis

The configuration and operational strategies of hybrid charging and hydrogen refuelling microgrids may vary in real-world applications. These design aspects impact total energy costs and decarbonisation potential. Therefore, our study includes a microgrid configuration and operational scenario analysis. To study the influences of design, dimensioning and operation strategies of the microgrid, we propose an optimisation study in which we vary the power and capacity of the BESS and HSS configurations as well as the operating strategy of power purchase and feed-in from and to the public grid. We define scenarios that cover different operational strategies and different time horizons. For example, we consider different years with individual data to analyse different charging demands. Operational strategies cover various forms of electricity procurement and feed-in.

We illustrate the relationship between individual optimisations of different BESS and HSS configurations with respect to the scenario analysis in Fig. 2. The BESS configurations $\{0, 1, \cdots, m\}$ include rated charging power and the total BESS energy capacity, the HSS configurations $\{0, 1, \cdots, n\}$ include rated power for the EL and FC as well as storage capacity for the HST. We number the configurations according to the increasing power and storage capacity of the BESS and the HSS. Thereby, we find the highest energy storage potential in the combination of HSS configuration n and BESS configuration m. Besides the configurational design, we define scenarios $\{1, 2, \cdots, s\}$ representing different operation strategies regarding power purchase and feed-in opportunity to the public grid. We vary electricity prices, feed-in tariffs, the electricity generation from the on-site PV plant, and overall customer demand for charging and hydrogen refuelling. We conduct a complete enumeration of n HSS configurations, m BESS configurations and s scenarios resulting in $(n\cdot m\cdot s)$ single optimisation instances. This procedure allows us to understand the influence of design and operation

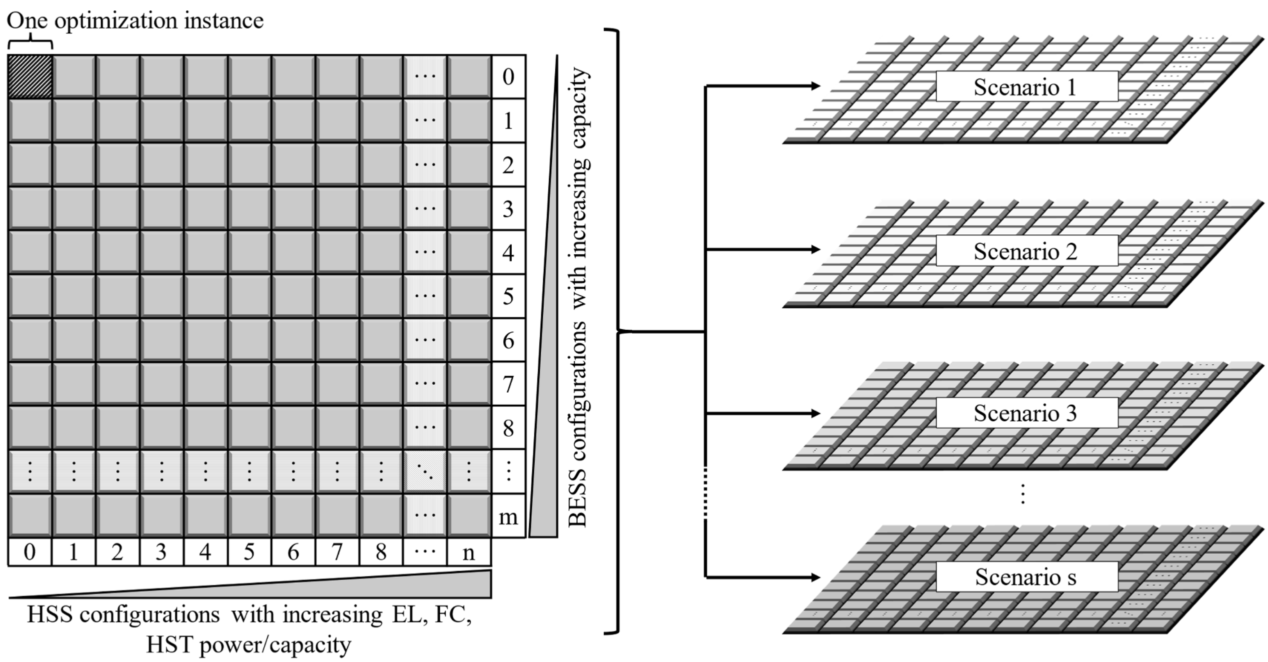

Fig. 2. Illustration of the relationship between individual optimisations of different BESS and HSS configurations and the scenario analysis. A set of different configurations are defined for both BESS and HSS, where configuration "0" represents no implementation of BESS and the lowest possible sizing of the HSS. Each combination of different BESS and HSS configurations is optimised individually. This procedure is repeated for a set of different scenarios.

on economic performance and decarbonisation potential.

3.4. Evaluation of decarbonisation potential

We determine relative and absolute indicators for GHG emissions and the decarbonisation potential *dcp* of BEV charging and FCEV hydrogen refuelling operation. All data and results on GHG emissions are given in CO_2-equivalents. To promote the decarbonisation potential of road transportation, hydrogen production and BESS charging should operate powerful during periods of high PV generation and during periods with a high share of RES in the electricity mix and a low emission factor. In contrast, high loads on the EL and high BESS charging, and thus the procurement of electricity, should be avoided if electricity from fossil sources such as coal with a high emission factor must be drawn from the grid. To evaluate the GHG impact on charging services and hydrogen refuelling provided in the microgrid, we determine the associated GHG share of purchased grid electricity $\overline{e}_t^{grid}$ for each time step t. Grid electricity emissions $\overline{e}_t^{grid}$ are based on the hourly feed-in capacities $P_{p,t}^{feed-in}[MW]$ of different types of energy sources $p \in P$ in the power system and the emission factors $e_p[gCO_2-eq/kWh]$ for each energy resource type [88]. Thus, for each kilowatt-hour drawn from the public grid, a corresponding relative GHG content $\overline{e}_t^{grid}[gCO_2-eq/kWh]$ is allocated (cf. equation (25)). Based on this relative emission factor, the total emissions associated with the consumption of grid electricity can be quantified. We calculate the average microgrid emission factor $\overline{e}^{MG}$ based on the emissions from grid-related energy together with PV system-related energy (cf. equation (26)). We then use the average emission factor to determine the GHG impact of produced hydrogen and provided charging services and thus, the decarbonisation potential for BEV and FCEV.

$$\overline{e}_t^{grid} = \frac{\sum_{p\in P} P_{p,t}^{feed-in} \cdot e_p}{\sum_{p\in P} P_{p,t}^{feed-in}} \quad \forall t \in T \tag{25}$$

$$\overline{e}^{MG} = \frac{\sum_{t=1}^{T} \left(P_t^{grid,in} \cdot \overline{e}_t^{grid} + P_t^{PV} \cdot e^{PV}\right)}{\sum_{t=1}^{T} \left(P_t^{grid,in} + P_t^{PV}\right)} \tag{26}$$

We assume a shift from ICE to BEVs in private transport and FCEVs in long-range heavy-duty trucks as a baseline. For each vehicle type, we consider the well-to-wheel GHG emissions in CO_2 equivalents per 100 km and include all GHG emissions released during supply and conversion of energy sources into electricity and fuels. BEV emissions include the average microgrid emission factor used for charging and the electricity consumption per 100 km $E^{BEV,ch}$ (cf. equation (27)). FCEV emissions also include the average microgrid emission factor, the relative energy consumption of the EL P^{EL} to produce hydrogen and the hydrogen consumption per 100 km $V^{FCEV,rf}$ (cf. equation (28)).

$$dcp^{BEV} = 1 - \frac{\overline{e}^{MG} \cdot E^{BEV,ch}}{e^{ICE,car}} \tag{27}$$

$$dcp^{FCEV} = 1 - \frac{\overline{e}^{MG} \cdot P^{EL} \cdot V^{FCEV,rf}}{e^{ICE,truck}} \tag{28}$$

As we analyse different microgrid configurations and operational strategy scenarios in the optimisation study, the decarbonisation potential is determined for all combinations of BESS and HSS configurations and scenarios.

4. Case study

4.1. Real-world mobility hub

We apply our methodological research design in a case study using real-world data. Therefore, an existing fast charging hub near the highly frequented highway A8 in southern Germany is a representative location. Due to its affiliation to the Ten-T core network [89], this location meets the requirements proposed in the Fit-for-55 package and thus ensures replicability due to the expansion of the European charging and hydrogen refuelling network. In addition to individual electrified passenger transportation, hydrogen-powered heavy-duty road transportation can also be expected at the location in the future due to the highly frequented highway and neighbouring industrial facilities.

Table 2
Overview of the optimisation scenarios used in the optimisation study.

Scenario	Year	Operational strategy
Scenario 1	2019	Market participation with Day-Ahead electricity procurement and feed-in prices.
Scenario 2	2019	Restricted market participation with Day-Ahead electricity procurement only, no feed-in to the public grid to optimise self-consumption.
Scenario 3	2020	Market participation with Day-Ahead electricity procurement and feed-in prices.
Scenario 4	2020	Restricted market participation with Day-Ahead electricity procurement only, no feed-in to the public grid to optimise self-consumption.
Scenario 5	2021	Market participation with Day-Ahead electricity procurement and feed-in prices.
Scenario 6	2021	Restricted market participation with Day-Ahead electricity procurement only, no feed-in to the public grid to optimise self-consumption.

4.2. *Scenario analysis*

We analyse the influence of two different operational strategies - Day-Ahead market participation and self-consumption optimisation without feed-in to the public grid - in three consecutive years – 2019, 2020 and 2021. This results in six scenarios listed in Table 2. We choose these years because we can observe varying traffic volumes and therefore charging and hydrogen refuelling demand due to the COVID-19 shutdowns in Germany. Beside the demand, the input data for electricity prices and feed-in profiles of the PV system, also differ between 2019, 2020 and 2021.

Based on real-world traffic flows, we model the charging and hydrogen refuelling demand for 365 days using quarter-hourly data from a highway traffic counting station near the designated location of the mobility hub in Zusmarshausen in southern Germany [90]. First, we extract the absolute number of hourly counted passenger cars and trucks from the BASt dataset. To determine the share of BEV and FCEV in the total traffic volume we use the BEV market penetration rate in Germany of 0.2 % for 2019 [91], 0.3 % for 2020 [92] and 0.6 % for 2021 [93] and assume that 0.1 % of all heavy-duty vehicles are FCEV in the scenarios. Finally, we assume a 70% charging/refuelling probability due to limited charging/hydrogen refuelling alternatives at this highway section. In Fig. 3, we illustrate the number of arriving BEV and FCEV for all years on the y-axis, whereby we separate the year on monthly basis on the x-axis. Based on the number of incoming vehicles, we assume that each arriving BEV charges for 30 min with a constant charging power of 150 kW and each FCEV heavy-duty truck refuels 180 Nm^3 hydrogen.

In addition, each scenario contains annual data on the electricity generated by the on-site PV system within the microgrid. Therefore, we use a PV module with 3,031 modules generating 330 W each [94], resulting in a total generation capacity of 1 MWp. As the PV systems power output is weather dependent, we use quarter-hourly irradiation and ambient temperature data from [95] to calculate the PV power output for all quarter-hours in 2019, 2020 and 2021.

In the scenarios with Day-Ahead market participation, additional feed-in revenues are generated through price-controlled use of the energy storage systems. In the scenarios with restricted market participation with Day-Ahead electricity procurement only, the optimisation aims to maximise self-consumption via the PV system. We list the data for economic parameters and their use in the respective scenarios in Table 3. Combining all six scenarios with each of the eleven BESS and HSS configurations results in 726 different optimisation instances which we implemented and solved with IBM ILOG CPLEX Optimisation Studio.

To determine the decarbonisation potential for passenger cars and heavy-duty trucks, we use the average well-to-wheel GHG emissions of passenger cars and trucks with ICE in Germany as a baseline. BEV electricity consumption per 100 km is based on the analysis of real-world energy consumption for 179 BEVs. The data and references for ICE vehicle emissions and electricity and hydrogen consumption are listed in Table 4.

4.3. *Configurations and parameterisation*

The parametrisation of the BESS contains the capacity and rated charging and discharging power for the technical configurations of the BESS unit. We model eleven BESS configurations, whereas configuration #0 corresponds to no installation of a BESS and configurations #1 to #10 cover a tenfold increase in capacity from 200 kWh to 2000 kWh, as listed in Table 5. For BESS's power to energy ratio, we adopt a conservative estimate of 0.5 in line with Hesse et al. [105].

We consider equal charging and discharging efficiencies, operating ranges, and initial states of charge for all BESS configurations. We limit the operation of the BESS between an SoC of 0.15 and 0.95, analogous to

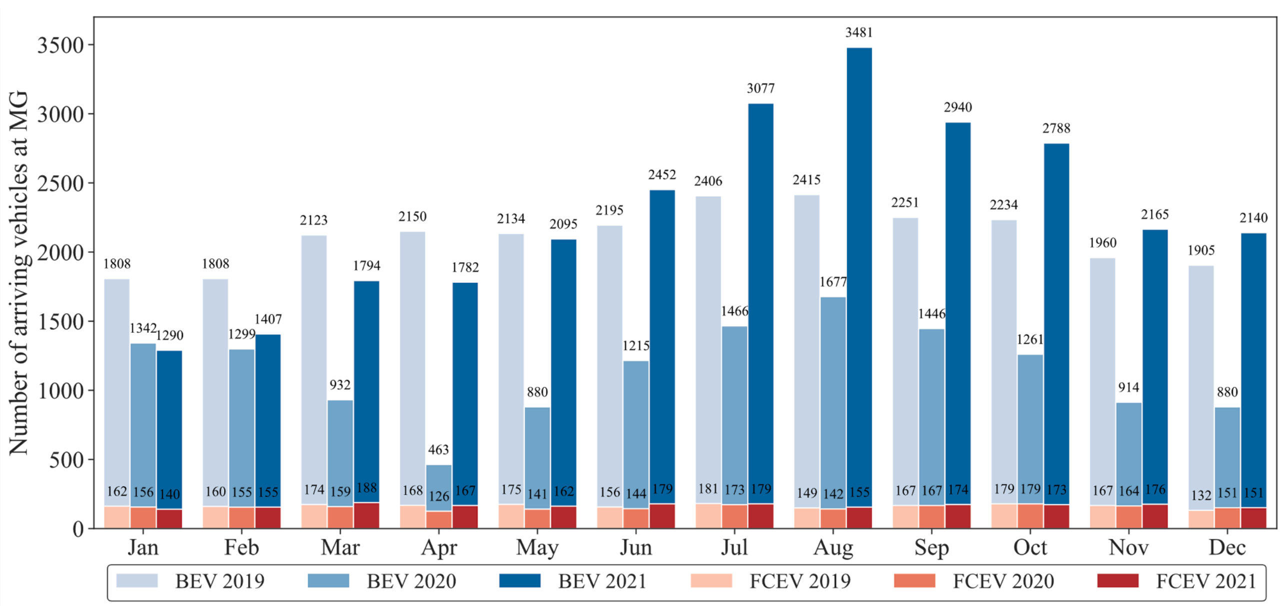

Fig. 3. Visualisation of incoming BEVs and FCEV volume derived from real-world traffic volumes during the years 2019, 2020 and 2021 registered at the counting station 9013 Zusmarshausen. Data: [90].

Table 3
Model parameters included in scenario data sets, including Day-Ahead prices, demand charge rates, feed-in tariffs and GHG emissions associated with grid electricity.

Parameter	Value	Description	Unit	Application in scenario	Reference
$EP_t^{in,2019}$ $EP^{out,2019}$	Day-Ahead time-series	Day-Ahead electricity market price time-series for 2019	$[EUR/kWh]$	Scenario 1, 2 Scenario 1	[96]
$EP^{dcr,2019}$	95.17	Demand charge rate 2019	$[EUR/kW\text{p.a.}]$	Scenario 1, 2	[97]
$\overline{e}_t^{grid,2019}$	Grid-emissions time-series	GHG emission content associated with grid electricity 2019	$[gCO_2-eq/kWh]$	Scenario 1, 2	[88,98]
$EP_t^{in,2020}$ $EP^{out,2020}$	Day-Ahead time-series	Day-Ahead electricity market price time-series for 2020	$[EUR/kWh]$	Scenario 3, 4 Scenario 3	[96]
$EP^{dcr,2020}$	98.57	Demand charge rate 2020	$[EUR/kW\text{p.a.}]$	Scenario 3, 4	[99]
$\overline{e}_t^{grid,2020}$	Grid-emissions time-series	GHG emission content associated with grid electricity 2020	$[gCO_2-eq/kWh]$	Scenario 3, 4	[88,98]
$EP_t^{in,2021}$ $EP^{out,2021}$	Day-Ahead time-series	Day-Ahead electricity market price time-series for 2021	$[EUR/kWh]$	Scenario 5, 6 Scenario 5	[96]
$EP^{dcr,2021}$	106.03	Demand charge rate 2021	$[EUR/kW\text{p.a.}]$	Scenario 5, 6	[100]
$\overline{e}_t^{grid,2021}$	Grid-emissions time-series	GHG emission content associated with grid electricity 2021	$[gCO_2-eq/kWh]$	Scenario 5, 6	[88,98]

Table 4
Data used to determine the decarbonisation potential of BEV and FCEV.

Parameter	Value	Unit	Reference
$e^{ICE,car}$	15,300	$[g\ CO_2-eq/100\ km]$	[101]
$e^{ICE,truck}$	226,000	$[g\ CO_2-eq/100\ km]$	[102]
$E^{BEV,ch}$	18.4	$[kWh/100\ km]$	[103]
$V^{FCEV,rf}$	89.0	$[Nm^3/100\ km]$	[104]

Wang et al. [106]. For the initial value for the BESS SoC, we assume the minimal possible SoC (SOC_{ini}^{BESS}) of 0.15. The general technical parameters for all BESS configurations are listed in Table 6.

The parametrisation of the HSS covers all parameters that characterise EL and FC operation, the electricity output, as well as the HST. Similar to the BESS, we model eleven HSS configurations with increasing power and storage capacities. We limit the minimum hydrogen output of the EL to 20 % of the maximum hydrogen output to maintain a linear energy consumption per Nm^3 of hydrogen produced as stated in the parameter P^{EL}. Similarly, we limit the minimum operation of the FC to 20 % of the maximum output power of the FC. We increase the HST storage volume accordingly with increasing EL and FC capacity. Table 7 lists all values for all HSS configurations.

The efficiencies of the EL – 74 % - and the FC – 56 % - are represented in the variables P^{EL} and V^{FC} [109,110]. For every electricity unit (kWh) provided to the EL, 0.2083 Nm^3 hydrogen is produced. In the reconversion process via FC 1 Nm^3 leads to an electricity generation of approximately 2 kWh. Hence, using electricity to produce hydrogen and to reconvert it into electricity again results in an overall efficiency of 41.44 %, irrespective of the specific configuration. The electricity consumption to achieve demanded hydrogen pressure levels by the H_2PC is included in the efficiencies of the EL and the FC. In the scope of this paper, we consider constant ambient temperature. Consequently, the electricity consumption of the H_2PC in order to adjust hydrogen pressure to the fluctuating ambient temperature is not considered further. We assume that the HST is empty before the optimisation time horizon.

Table 6
Technical General parameters which are all applied for the 11 BESS configurations.

BESS-Parameter	Value	Reference
SOC_{min}^{BESS}	0.15	[106]
SOC_{max}^{BESS}	0.95	[106]
SOC_{ini}^{BESS}	0.15	own assumption
$SOC_{ch}^{BESS,tap}$	0.80	[107]
$SOC_{dis}^{BESS,tap}$	0.20	[107]
η_{ch}^{BESS}, η_{dis}^{BESS}	0.935	[108]

Therefore, we set the minimum storage volume to $V_{min}^{HST} = 0\ Nm^3$. Table 8 lists the values applied for the EL, FC and HST parameters for all eleven configurations.

5. Results

5.1. Validation of optimisation results

In the first phase of our analysis, we validate our optimisation results using exemplary real-world data along with our optimisation output. We implemented and solved the 726 instances of the optimisation study using IBM ILOG CPLEX Optimisation Studio on a system with 12 CPU cores with a clock speed up to 4.7 GHz and a 64 GB RAM. An exemplary period of three days for both summer and winter in 2019 is illustrated in Fig. 4 with the respective PV output power, BESS SoC and HST filling level. The charging and discharging behaviour of the BESS is influenced by the PV output power. In summer, we note that BESS is charged in periods with significant solar power output and discharged in periods with reduced PV power output. We also observe a higher HST filling level in summer for both operating strategies, which can be expected as the EL can utilise more PV power. In winter, the HST filling level tends to be considerably lower, regardless of the operating strategy as the PV power output is diminished. These observations confirm the economic

Table 5
Technical parameters including energy storage capacity and rated power for the 11 BESS configurations. Data based on own selection.

BESS configuration #	0	1	2	3	4	5	6	7	8	9	10
$P_{cap}^{BESS}[kWh]$	0	200	400	600	800	1,000	1,200	1,400	1,600	1,800	2,000
$P_{rated}^{BESS}[kW]$	0	100	200	300	400	500	600	700	800	900	1,000

Table 7
Technical parameters of the 11 different HSS configurations with increasing rated power of the EL and FC and increasing storage capacity of the HST.

HSS configuration #	0	1	2	3	4	5	6	7	8	9	10
$V^{EL}_{min}\,[Nm^3/h]$	12	14	16	18	20	22	24	26	28	30	32
$V^{EL}_{max}\,[Nm^3/h]$	60	70	80	90	100	110	120	130	140	150	160
$P^{FC}_{min}\,[kW]$	6	7	8	9	10	11	12	13	14	15	16
$P^{FC}_{max}\,[kW]$	30	35	40	45	50	55	60	65	70	75	80
$V^{HST}_{max}\,[Nm^3]$	30,000	35,000	40,000	45,000	50,000	55,000	60,000	65,000	70,000	75,000	80,000

Table 8
HSS-Parameters applied throughout different optimisation instances.

Parameter	Value	Unit	Reference
P^{EL}	4.80	$[kWh/Nm^3]$	[110]
V^{FC}	0.50	$[Nm^3/kWh]$	[109]
V^{HST}_{min}	0.00	$[Nm^3]$	assumption
V^{HST}_{ini}	0.00	$[Nm^3]$	assumption

logic to reduce total energy costs on which we based the optimisation objective, as the energy storage systems of both BESS and HSS are exploited to draw as much power as available from the on-site PV system within the microgrid.

5.2. *The economics of operating strategies and system configurations*

We first analyse the economics of each operating strategy and microgrid system configurations within the predefined scenarios, illustrated in a 6-by-4 matrix in Fig. 5. Each column depicts one scenario. The rows represent the total energy costs and their components per year, i.e., grid demand charges, volume-based electricity costs, and feed-in revenues. Each diagram plots the optimisation results for all BESS and HSS combinations, with the HSS configurations depicted on the x-axis and eleven line plots, each representing one BESS configuration.

We find that in all scenarios the annual total energy costs decrease with increasing BESS and HSS capacity and performance. Further, we observe that the annual total energy costs converge with increasing BESS and HSS rating and capacity. That means, at some point additional capacity results in no further significant cost savings. In both 2019 scenarios, the potential to reduce marginal total energy costs decreases with increasing BESS and HSS system power, converging to no further significant cost reduction at approximately 139,000 EUR. We observe the same trend of converging total energy costs in both 2020 and 2021 scenarios as BESS capacity increases. In contrast, there is no strong convergence of the total energy costs due to an expanding HSS system. While we see no significant differences in total energy costs between the Day-Ahead market participation and self-consumption optimisation in 2019, we find the contrary effect in 2020. By comparing all individual system combinations of BESS and HSS for both operating strategies in 2020, we determine an annual average decrease in total energy costs of 4,370 EUR, when participating in Day-Ahead marketing in contrast to optimising towards self-consumption. In 2021 this trend is even higher due to the more volatile Day-Ahead prices, and we identify an annual average decrease in total energy costs of 6,695 EUR.

Next, we analyse the load peak related annual demand charges. At first glance, there are no differences between the operating strategies in each year. Across all scenarios, the BESS contribute to lower grid demand charges by buffering and reducing peak loads. This effect on the demand charges converges with increasing BESS capacity in all four scenarios because, at some point, the BESS capacity exceeds the peak loads. In 2019, the 2,000 kWh BESS reduces the demand charges to roughly 40,000 EUR. Despite a slightly higher demand charge rate imposed by the grid operator in 2020, the BESS can contribute to cut demand charges to less than 35,000 EUR in both 2020 scenarios. With an even higher demand charge rate in both 2021 scenarios, BESS effectively reduces the annual demand charges to less than 40.000 EUR.

Following, we focus on the volume-based electricity costs. At first notice, the volume-based electricity costs are significantly lower in 2020 than in 2019 and significantly higher in 2021. The annual volume-based electricity costs range from 103,000 EUR to 113,000 EUR in 2019, 43,000 EUR to 68,000 EUR in 2020 and 124,000 EUR to 202,000 EUR in

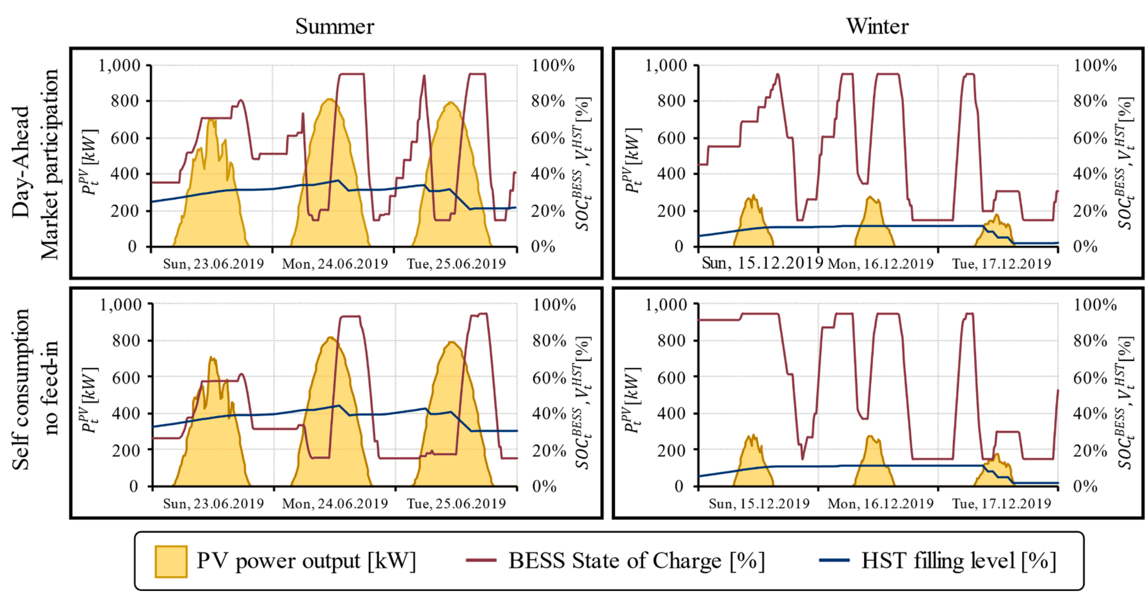

Fig. 4. Exemplary operational analysis of the proposed scheduling model considering PV power, BESS SoC and HST level for an exemplary time-period of three days for both summer and winter in 2019 applying BESS configuration #5 and HSS configuration #5.

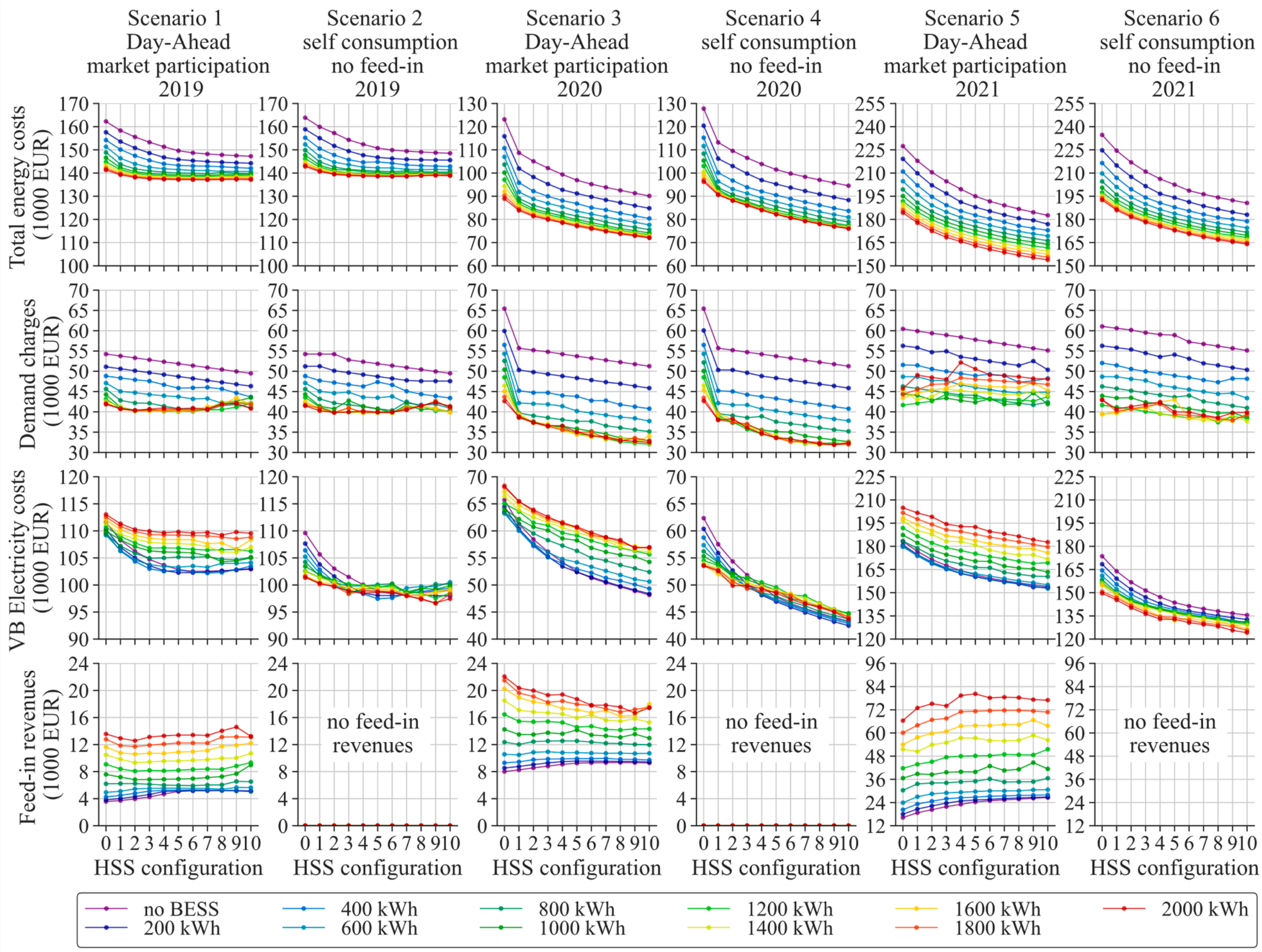

Fig. 5. Optimisation results for different BESS and HSS configurations and operational scenarios. The total costs are split up into the different cost components of the objective function.

2021 across both operational strategies. Unlike the total energy costs and the demand charges, the annual volume-based electricity costs increase through Day–Ahead market participation in all years with increasing BESS power and capacity. In the self-consumption scenarios without feed-in, we find that with the expansion of BESS and HSS, the annual volume-based electricity costs are significantly lower than in Day-Ahead market participation scenarios. However, applying the self-consumption optimisation in 2019 and 2020, increasing BESS capacity does not lead to further changes in the volume-based electricity costs. Through an expansion of the HSS, the volume-based electricity costs converge at approximately 100,000 EUR in 2019, while they continue to decrease in 2020 and 2021.

We further evaluate the realised feed-in revenues in the Day-Ahead market participation scenarios, where revenues are generated through electricity feed-in. Note that grid feed-in is avoided in the self-consumption scenarios and thus no revenue is generated. We observe that increasing BESS capacity and performance can generate more revenue through stronger electricity trading. Thereby, due to the symmetric price design between the electricity procurement price and feed-in compensation at the Day-Ahead market, the marginal benefit of BESS in the MG is highly evident. In 2019, feed-in revenues can reach up to 15,000 EUR, up to 22,000 EUR in 2020 and even 80,000 EUR in 2021. As the power of the EL, the FC, and the HST capacity increase, we see that no additional revenues are generated from the reconversion of hydrogen via the FC in 2019. In 2020 we can even observe that the feed-in revenues for large BESS decrease by scaling up the HSS. For example, the feed-in revenue is reduced by approximately 7,000 EUR from the smallest to the largest HSS using a 2000 kWh BESS. In contrast, in 2021, increasing HSS capacity initially yields higher feed-in revenues followed by no further growth with moderately sized HSS configurations.

5.3. Decarbonisation potential of road transportation

To analyse the decarbonisation potential of our MG, we illustrate the average GHG emission factors per kWh and the associated total GHG emissions for grid electricity procurement for all scenarios in Fig. 5. The structure is analogous to Fig. 6, except for the rows that now illustrate the average emission factor and total emissions associated with grid electricity procurement.

In the Day-Ahead market participation scenarios, additional BESS capacities increase the average emission factor within most instances. In addition, we observe overall higher average emission factors in 2019 than in 2020 and 2021. If we examine the largest HSS configuration for all years, the relative emission improvement in 2019 reaches only 10 $gCO_2 - eq/kWh$, while it rises to 18 $gCO_2 - eq/kWh$ in 2020 and 20 $gCO_2 - eq/kWh$ in 2021. Furthermore, in 2019 we observe that the average emission factor for growing HSS configurations remains fairly constant, e.g., at about 270 $gCO_2 - eq/kWh$ in the largest BESS configuration. In 2020, the average emission factor for larger HSS configurations continues to decrease, while in 2021, the reduction for moderate HSS configurations stagnates.

The results for the self-consumption operational strategy without feed-in opportunity differ. In 2019, 2020 and 2021 the average emission factor decreases with the expansion of the BESS considering the smallest

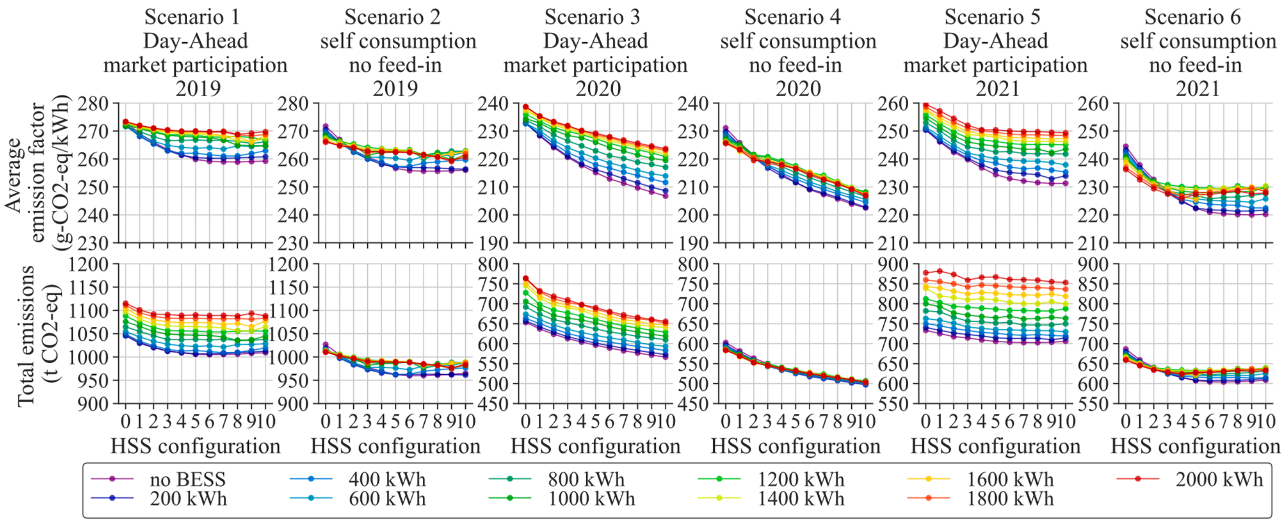

Fig. 6. Illustration of the average emission factors and the total associated GHG emissions for all microgrid configurations and operational strategies.

HSS configuration but increases when the HSS grows. In 2020, the average emission factor ranges from 191 gCO_2-eq/kWh in the best case to 226 gCO_2-eq/kWh in the worst case. Further, we note that while in 2020 an increase in HSS power and capacity leads to a significant reduction in average emission factors, in 2019 the marginal reduction of the emission factor converges to zero. In 2021 the total spread of average emission factors is higher than in previous years. For instance, for the largest HSS configuration, the spread between no BESS and the 2000 kWh BESS configuration is approximately 11 gCO_2-eq/kWh, comparing to 5 gCO_2-eq/kWh in 2019 and 8 gCO_2-eq/kWh in 2020.

Next, we analyse the annual total emissions associated with the procurement of grid electricity. Total emissions increase significantly with expanding the BESS capacity in all years within the Day-Ahead market participation strategy. In 2019 and 2021 we find that the total emissions converge with the enlargement of the HSS system, while in 2020, a further decrease in total emissions is achieved with the same operating strategy. In 2019, the annual total emissions range between 1,005 and 1,115 tons, in 2020 between 566 and 655 tons and in 2021 between 706 and 853 tons with Day–Ahead market participation operation. We also observe a total emission reduction potential in 2020 along with the HSS expansion. We observe a similar trend in 2021 for the initial expansion steps of the HSS. The results of the self-consumption operational strategy demonstrate that the total emissions associated with grid procurement do not differ significantly regarding changes of the BESS configurations. In this case, annual total emissions range from 959 to 1026 tons in 2019, from 497 to 602 tons in 2020 and from 604 to 686 tons in 2021.

Last, we focus on the decarbonisation potential of BEV charging and FCEV hydrogen refuelling at the microgrid in comparison to passenger cars and heavy-duty trucks with fossil fuel powered ICE. The average emission factor depends on the microgrid configuration and the operating strategy, which leads to different GHG emissions implied by charging services and hydrogen production. As a result, the decarbonisation potential of BEV and FCEV is significantly influenced. We depict the decarbonisation potential of both BEV and FCEV across all scenarios in Fig. 7. Once more, HSS configurations are depicted on the x-axis, while the y-axis from top to bottom gives the decarbonisation potential for BEV and FCEV. The columns address the years and the strategy scenarios, and each graph consists of eleven line plots representing one BESS configuration.

First, we observe that the decarbonisation potential is significantly smaller for FCEVs than for BEVs. While the decarbonisation potential for BEVs amounts 67.12 % in the minimum case and 75.63 % in the maximum case, the decarbonisation potential for FCEVs ranges between

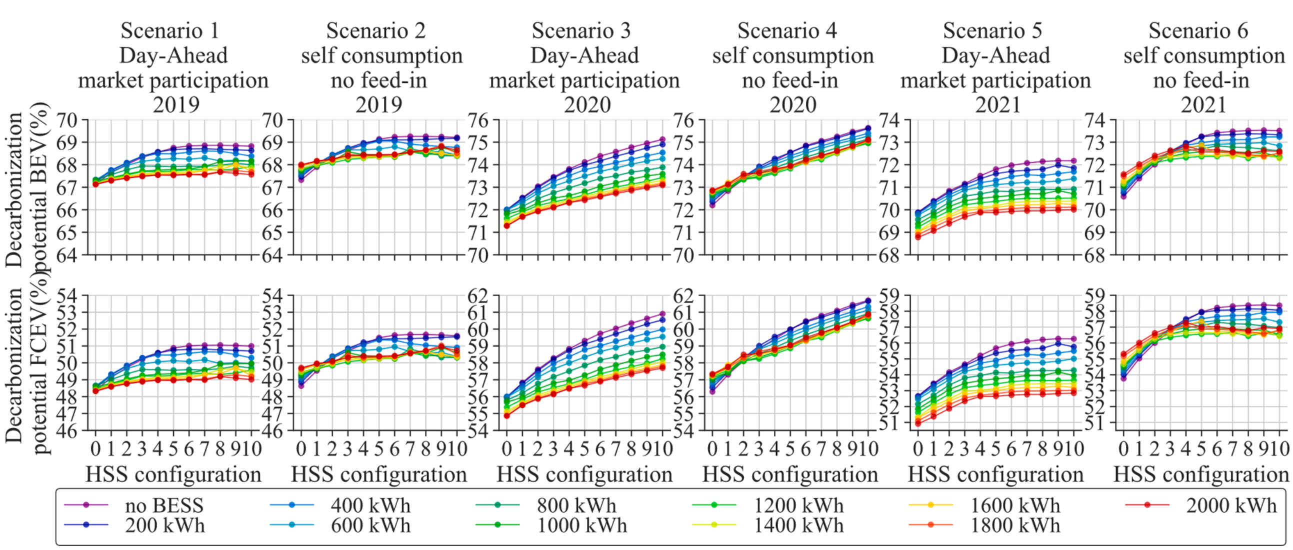

Fig. 7. Illustration of the decarbonisation potential of BEV and FCEV in comparison to passenger cars and heavy-duty trucks with fossil fuel powered ICE.

48.32 % and 61.69 %. In all three consecutive years, we find a clear reduction in the decarbonisation potential with expanding BESS capacities considering Day-Ahead market participation. In contrast, in the self-consumption scenarios we see an initial reversed effect for the HSS configurations #0 and #1 in 2019 and 2020 and for the HSS configurations #0, #1 and #2 in 2021 where the decarbonisation potential increases as the storage capacity of the BESS increases. Like the average emission factor and the total emissions, the decarbonisation potential for BEVs and FCEVs in 2019 converges through the Day-Ahead market participation. Yet, with the same operating strategy in 2020, we observe a continuous increase in the decarbonisation potential for both vehicle types. In 2021, the increase of the decarbonisation potential for both vehicle types concludes halfway through the analysed HSS configuration stages.

Comparing the decarbonisation potential in 2019 (Scenario 1 & 2) and 2020 (Scenario 3 & 4), we observe a significant increase for both vehicle types, BEVs and FCEVs. However, in 2021 (Scenario 5 and 6), the decarbonisation potential is reduced compared to 2020, but still reaches an increased level compared to 2019. The BEV decarbonisation potential ranges from 67.12 % to 69.25 % in 2019, from 71.28 % to 75.63 % in 2020 and from 68.77 % to 73.53 % in 2021, while the FCEV decarbonisation potential ranges from 48.32 % to 51.67 % in 2019, from 54.86 % to 61.69 % in 2020 and from 50.91 % to 58.39 % in 2021. Furthermore, we find that the decarbonisation potential is higher for the same BESS and HSS configuration in the scenarios with optimisation towards self-consumption.

6. Discussion

Our results show that BESS's application in a hybrid charging and hydrogen refuelling station microgrid reduces demand charges and overall energy costs. Therefore, the BESS reduces peak loads by flattening the electricity demand from the grid over the year. The BESS stores surplus electricity from the PV system and charges during low electricity prices. Without electricity feed-in, the BESS is solely dedicated to optimise self-consumption, whereas, through Day-Ahead market participation, additional revenues are generated through electricity trading. Consequently, total energy costs are lower in both years. However, the differences in 2019 with higher BEV charging demand are rather marginal between the operating strategies, why microgrid operators may be indifferent when deciding on the operating strategy for economic reasons. In 2020 and 2021 the results indicate that electricity marketing will be more attractive. However, since the operational strategy of Day-Ahead market participation does not perform worse in either scenario, it is preferable from an economic perspective to switch to this operational strategy.

The results demonstrate that the total annual energy costs decrease, and the decarbonisation potential increases when the performance and capacity of the HSS system grows. The EL is the major electricity consumer within the microgrid, and at higher production capacities, more hydrogen can be produced during periods with high local renewable energy production through PV or when Day-Ahead electricity prices are low. Especially through the increase of the storage capacity, a continuous production of hydrogen is not necessary to maintain sufficient levels of hydrogen in the HST to cover the minimum hydrogen demand. Non-continuous production reduces the percentage utilisation of the EL over the year. Since high power microgrid components imply increasing initial investments, investors and microgrid operators may generally share a high economic interest in high capacity utilisation of EL and FC [111]. Further analysis reveals that the annual utilisation of the EL (solid line) decreases with higher capacity while FC utilisation (dashed line) remains rather low in all cases (cf. Fig. 8). We note no significant deviations in EL utilisation and only a minor influence on the FC, as the charging and hydrogen demand remains constant among the various BESS configurations and operational strategies. While low utilisation may be less profitable from the microgrid investor's perspective, operating HSS with high production capacities can still lead to further total energy cost reductions in microgrid operation. In this case, the EL can exploit seasonal effects resulting from RES power generation, like high surplus energy output of the PV system, especially in times with lower charging demand.

Aiming to operate the EL more constantly and thus increasing the annual utilisation causes an increase in the associated emissions. It may be environmentally preferable to increase the flexibility of operation by deploying high power EL and thus utilise the availability of local RES, especially in times of low electricity prices. In this context, microgrid operators need to take the maximum supply power via the GCP into account, which represents a potential bottleneck in the case of very powerful ELs. However, the high investment costs combined with the low utilisation of the high-capacity ELs may discourage potential investors. While FC utilisation is rather low in most scenarios, we observe an increase in FC utilisation in the self-consumption strategy in 2020 using small HSS configurations. Due to lower demand in this scenario, abundant surplus electricity output from the PV system is available for hydrogen production, which makes it reasonable to convert excess hydrogen into electricity to power charging services in periods with less available renewable energy. Apart from scenarios like these, the operation of the FC is rather uneconomical due to high efficiency losses in the process chain from the generation to the reconversion of hydrogen into electricity [112]. From this, we deduce that FC power should not be oversized when integrating FC into hybrid charging and hydrogen refuelling stations.

Our decarbonisation analysis reveals that a higher decarbonisation potential can be realised through self-consumption optimisation

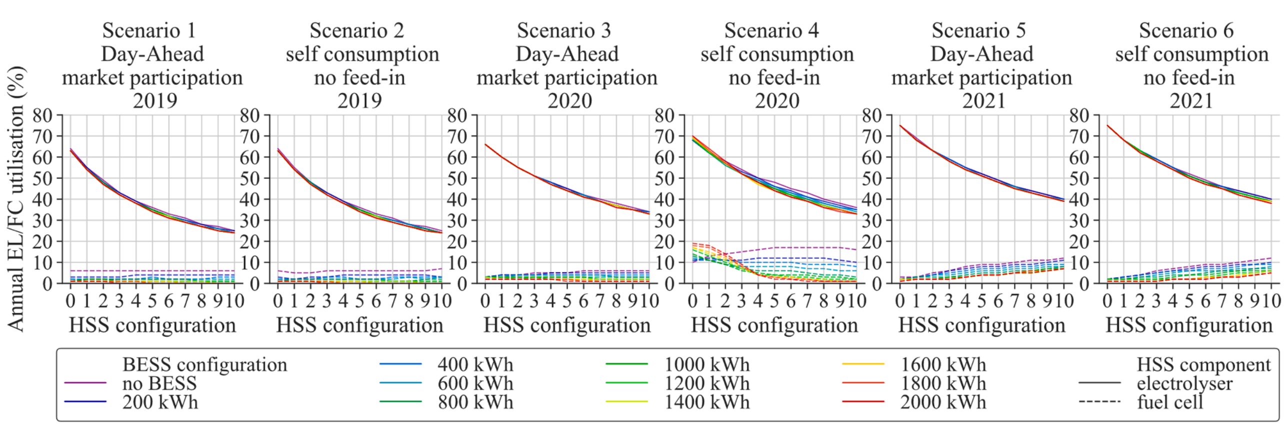

Fig. 8. Illustration of the electrolyser and fuel cell annual utilisation. HSS configurations are depicted on the y-axis. BESS configurations are distinguishable between line plots. Solid lines indicate results for EL and dashed lines for FC.

compared to participation in the Day-Ahead market. The main difference between the operating strategies is the higher electricity volume procurement due to the marketing potential within the Day-Ahead market participation strategy. The higher volume of electricity purchased from the grid increases the average emission factor, as grid electricity has a significantly higher average associated emission factor than on-site PV electricity. In 2020, the decarbonisation potential is significantly larger than in 2019. In 2020, the total energy demand is considerably lower due to the reduced traffic volume and thus lower demand for charging services. In this case, less electricity must be drawn from the grid, and proportionally more electricity is used from the PV system. This has a beneficial influence on total energy costs and total emissions, which is also reflected in a lower emission factor in both scenarios for 2020. In 2021, the total electricity charging demand is considerably higher than in the previous year, yet the decarbonisation potential of both BEVs and FCEVs increased compared to 2020.

Our results reveal that the cost-effectiveness of designing and operating microgrids for hybrid charging and hydrogen refuelling stations is not aligned with further progress on decarbonisation. We wouldńt anticipate this effect, as feed-in from RES in Germany is prioritised over fossil power plants by the merit order model [113]. Accordingly, we expect that in both self-consumption scenarios with high energy storage capacities, more low-cost electricity from RES is procured and thus total costs and emissions can be reduced simultaneously. For example, the BESS can compensate peak loads and balance electricity demand from the public grid throughout the year. Feed-in revenues are generated by exploiting price fluctuations when participating in the Day-Ahead market. In this context, electricity associated with higher emission factors is procured and reduces the decarbonisation potential. Throughout all scenarios, we find a reduction in decarbonisation potential with an increase in BESS capacity while total annual costs can be reduced. To analyse this economic and ecologic mismatch, we further investigate the relation between costs for the microgrid operator and the emissions associated with grid electricity.

We plot the Day-Ahead electricity prices and the emission factors for 2019, 2020 and 2021 in Fig. 9 and provide statistical descriptors for average values, deviation and correlation in Table 9. A correlation between Day-Ahead Spot prices and the emission factor is strongly evident with a slightly higher correlation in 2020 than 2019. Day-Ahead electricity prices are on average 7.20 EUR/MWh lower in 2020 than in 2019. In 2021, the average Day-Ahead Price reached approximately-three times the level of the previous year. The deviation of prices grew throughout the years analysed, with a deviation nearly-five times higher in 2021 than was observed in 2019. Furthermore, the average emission factor for grid electricity procurement is approximately 46 $gCO_2 - eq/kWh$ lower in 2020 than in the year before, but roughly 8 $gCO_2 - eq/kWh$ higher in 2021. We observe a positive correlation between Day-Ahead electricity prices and associated emission factors in 2019, 2020 and 2021. This correlation is even higher in 2020 with a value of 0.7605 than in 2019 with 0.7184. However, the correlation of the previous years is reduced in 2021 with a value of 0.5323.

The positive correlation implies that it is favourable to align electricity purchases with low prices and low GHG emissions from an economic and decarbonisation perspective. Therefore, with the correlation of prices and emissions, a low cost and low GHG operation of hybrid charging and hydrogen refuelling microgrids could be achieved simultaneously without trade-offs. An increase in CO_2 pricing is likely to lead to a higher correlation between electricity prices and emission factors in the future. However, the reduction of the peak load and thus grid demand charges bear a significant economic benefit. An increase in the annual peak load is only economically viable, if each kW of additional peak load is accompanied by a total energy cost reduction that is higher than the amount of the demand charge rate imposed by the grid operator, which in our study is 95.17 EUR/kWp.a. in 2019, 98.57 EUR/kWp.a. in 2020 and 106.03 EUR/kWp.a. in 2021. Yet, our results reveal that it pays off from an economic perspective to reduce the load peaks and thus to choose a steady electricity inflow from the grid rather than the increasing peak load to benefit from high volume electricity procurement in low-price periods. Consequently, the effect of the positive correlation of electricity prices and emission factors in the Day-Ahead market is not realised for hybrid charging and hydrogen refuelling microgrid operation. As a result, the achieved decarbonisation potential decreases in both scenarios without feed-in. Nevertheless, minor improvements at an individual hybrid charging and hydrogen refuelling station result in major GHG emission savings at scale.

7. Conclusion

In this article, we investigated the sustainable design and operation of grid-connected hybrid hydrogen refuelling and electric vehicle charging microgrids in Germany for decarbonising road transportation. We conducted an optimisation study to analyse the influences of varying microgrid configurations and different operating strategies on the operational costs and decarbonisation potential. Our results reveal that the choice of microgrid configuration design, sizing and operational strategy strongly influences total energy costs and the decarbonisation potential of BEV charging and FCEV refuelling. Results indicate a decarbonisation potential of 67.12 % in the minimum case and 75.32 % in the maximum case for BEV charging and likewise 48.32 % and 61.69 % for FCEV refuelling in comparison to refuel passenger cars and heavy-duty vehicles with ICE. While high BESS capacity can significantly reduce total energy costs, GHG emissions increase. High performance power of EL, FC as well as HST storage capacity results in a reduction of the total energy costs and an improvement of the realised

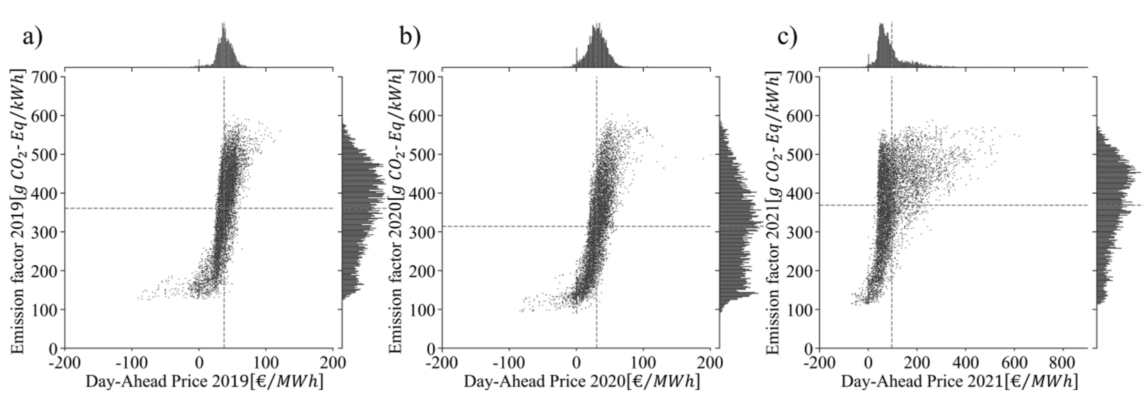

Fig. 9. Illustration of the relationship between Day-Ahead prices and GHG emission factors of the years 2019 (a) and 2020 (b). Each Figure show the Day-Ahead prices on the x-axis and the emission factors on the y–axis. At the top and right of each graph, we include a histogram illustrating the distribution of prices and emissions. We include both the mean value and the standard deviation for prices and emission factors. Data: (ENTSO-E, 2021b, 2021a; Lauf et al., 2021).

Table 9
Statistical data on Day-Ahead prices for the German bidding zone and emission factors associated with electricity procurement in Germany.

Statistical descriptor	2019	2020	2021	Unit	Reference
Average Day Ahead Price	37.67	30.47	96.85	[€/MWh]	[96]
Standard deviation Day Ahead Price	15.52	17.50	73.68	[€/MWh]	[96]
Average emission factor	360.72	314.24	368.73	[$gCO_2 - eq/kWh$]	[88,98]
Standard deviation emission factor	104.71	112.95	106.45	[$gCO_2 - eq/kWh$]	[88,98]
Correlation Day-Ahead prices and emission factors	0.7184	0.7605	0.5323	[−]	[88,96,98]

decarbonisation of BEV and FCEV, but at the same time, the total annual utilisation rate of the HSS decreases. Further, we deduced that the simultaneous maximisation of cost efficiency and high decarbonisation of hybrid charging and hydrogen refuelling stations is discouraged by current grid demand charge regulation.

The findings of this study lead to several implications for policy, practice, and research. First, we identified grid demand charges as a major factor preventing the benefits of the positive correlation of Day-Ahead electricity prices and emission factors for simultaneous economic and ecological operation in our case study. While high energy storage capacities are mostly associated with decreasing GHG emissions, significantly high grid demand charges hinder simultaneous economic and ecologic operation in a Day-Ahead marketing scenario. Therefore, we argue for regulatory reform of grid charges. We propose that the assessment basis for demand charges should be changed to shorter time intervals. Here, we suggest a weekly or daily assessment of the load peaks for grid demand charges to benefit from economic and decarbonisation potentials within low electricity prices and emission factors of grid electricity procurement. This modification can enable decentralised electrolysis systems to benefit from a higher load peak during RES oversupply periods in the public grid. Thus, procuring higher electricity volumes when prices and associated GHG emissions are low to produce large quantities of hydrogen. Consequently, the microgrid operator can reduce hydrogen production in times of high electricity prices with a comparatively high share of emissions.

Second, our results provide guidance for policymakers on infrastructure development and thus subsidising similar charging and hydrogen refuelling microgrids in the future. As the Fit-for-55 regulatory proposal aims to establish infrastructure for decarbonised mobility, policymakers should promote economically and ecologically viable microgrids. Besides subsidising infrastructure, tax incentives during operation may accelerate deployment of charging and hydrogen refuelling microgrids at scale and promote market ramp up of BEV and FCEV to achieve decarbonisation in road transportation.

Third, decarbonisation of electricity supply by expanding RES generation capabilities will be a key driver of BEV and FCEV decarbonisation potential when charging, and hydrogen generation are powered by electricity drawn from the grid. As grid electricity is coupled to lower GHG emissions per kWh, the benefits of electricity and hydrogen as fossil fuel substitutes increase. Therefore, installing power plants with low GHG impacts such as PV arrays and wind turbines should not only be a main target of policymakers because of economic considerations but should also be integrated cross-sectoral with transportation electrification. As motorways often neighbour large open spaces, there are significant synergies to install high-RES generation capacities at hybrid charging and hydrogen refuelling stations. Further, our results reveal design and operational guidance for microgrid operators. Microgrid investors and operators should exploit the high cost reduction potential of higher BESS capacity to improve economic viability. In addition, the operating strategy of participating in the Day-Ahead market offers an economic advantage for large corporations with access to the Day-Ahead market. In contrast, operators of charging and hydrogen refuelling stations without access to the Day-Ahead market may adopt the operating strategy of self-consumption optimisation. This strategy may prove beneficial if the company's core activity does not involve electricity marketing or if company resources cannot be dedicated to this purpose.

Fourth, we focused on the variable electricity market prices of the German day-ahead bidding zone and German regulation. Future studies could examine the impact of participation in other or multiple markets, such as intraday or ancillary services markets, on microgrid design and operation. Also, transferring our study design to other regions with different regulatory or market characteristics, analysing external effects of different shares of the electricity mix or EV / FCEV penetration rates, or considering long-term electricity price or mobility forecasts could provide valuable insights for researchers, practitioners, or policymakers.

Naturally, this study is subject to some limitations as any research endeavour. However, these limitations give rise to future research. First, assuming complete information on electricity prices, charging and hydrogen demand, and actual PV generation capacity, we could determine the optimal scheduling for the microgrid configurations with both operational strategies presented, which may not be possible under uncertain conditions. Microgrid operators require high-quality data forecasts on RES availability and charging/hydrogen demand to operate hybrid charging and hydrogen refuelling stations profitable under uncertainty. In this context, data-driven AI methods showing high predictive performance in other domains could be suitable and addressed in further studies. Second, we have not considered capital expenditure in our economic analysis as investment incentives are already considered in current hydrogen strategies. However, combining an operational and investment perspective may be of interest for further research. Against the backdrop of limited financial resources, policymakers may leverage further potential of a holistic subsidy strategy.

CRediT authorship contribution statement

Robert Förster: Conceptualization, Methodology, Software, Formal analysis, Investigation, Data curation, Writing – original draft, Writing – review & editing, Visualization, Project administration. **Matthias Kaiser:** Conceptualization, Methodology, Formal analysis, Writing – original draft, Writing – review & editing, Supervision. **Simon Wenninger:** Conceptualization, Methodology, Formal analysis, Writing – original draft, Writing – review & editing, Supervision.

Declaration of Competing Interest

The authors declare that they have no known competing financial interests or personal relationships that could have appeared to influence the work reported in this paper.

Data availability

Data will be made available on request.

Acknowledgement

The authors gratefully acknowledge the financial support of the

Bavarian Ministry of Economic Affairs, Regional Development and Energy for the Project "ODH@SIZ" (Grant No. IUK-1812-0020//1UK610/004) as well as the German Federal Ministry of Education and Research (BMBF) and the project supervision of the project management organization Projektträger Jülich (PtJ) for the Kopernikus-project "SynErgie" (Grant No. 03SFK3A3-2; 03SFK3T2-2). Responsibility for the contents remains solely with the authors.

References

[1] Forster PM, Forster HI, Evans MJ, Gidden MJ, Jones CD, Keller CA, et al. Current and future global climate impacts resulting from COVID-19. Nat Clim Chang 2020;10(10):913–9.
[2] European Commission. Fit for 55: delivering the EU's 2030 climate target on the way to climate neutrality. Brussels; 2021.
[3] International Energy Agency (IEA). The role of CCUS in low-carbon power systems. [November 17, 2022]; Available from: https://www.iea.org/reports/the-role-of-ccus-in-low-carbon-power-systems.
[4] Morrison G, Stevens J, Joseck F. Relative economic competitiveness of light-duty battery electric and fuel cell electric vehicles. Transport Res Part C: Emerg Technol 2018;87(5):183–96.
[5] Michalski J, Poltrum M, Bünger U. The role of renewable fuel supply in the transport sector in a future decarbonized energy system. Int J Hydrogen Energy 2019;44(25):12554–65.
[6] Eberle U, von Helmolt R. Sustainable transportation based on electric vehicle concepts: a brief overview. Energy Environ Sci 2010;3(6):689.
[7] Çabukoglu E, Georges G, Küng L, Pareschi G, Boulouchos K. Fuel cell electric vehicles: an option to decarbonize heavy-duty transport? Results from a Swiss case-study. Transp Res Part D: Transp Environ 2019;70(2):35–48.
[8] European Commission. REPowerEU: a plan to rapidly reduce dependence on Russian fossil fuels and fast forward the green transition. [November 27, 2022]; Available from: https://ec.europa.eu/commission/presscorner/detail/en/IP_22_3131.
[9] Greene DL, Ogden JM, Lin Z. Challenges in the designing, planning and deployment of hydrogen refueling infrastructure for fuel cell electric vehicles. eTransportation 2020;6(1):100086.
[10] Springel K. Essays in industrial organization and environmental economics: network externality and subsidy structure in two-sided markets: evidence from electric vehicle incentives. Dissertation. Berkley; 2017.
[11] Shi L, Hao Y, Lv S, Cipcigan L, Liang J. A comprehensive charging network planning scheme for promoting EV charging infrastructure considering the Chicken-Eggs dilemma. Res Transp Econ 2020;21(3):100837.
[12] European Court of Auditors (ECA). Infrastructure for charging electric vehicles: more charging stations but uneven deployment makes travel across the EU complicated. Luxembourg; 2021.
[13] European Commission. Proposal for a regulation of the European Parliament and of the Council on the deployment of alternative fuels infrastructure, and repealing Directive 2014,94. Brussels: EU of the European Parliament and of the Council; 2021.
[14] European Parliament. Fit for 55: Transport MEPs want car-recharging stations every 60 km; Available from: https://www.europarl.europa.eu/news/en/press-room/20221003IPR42118/fit-for-55-transport-meps-want-car-recharging-stations-every-60-km.
[15] Siskos P, Zazias G, Petropoulos A, Evangelopoulou S, Capros P. Implications of delaying transport decarbonisation in the EU: a systems analysis using the PRIMES model. Energy Policy 2018;121:48–60.
[16] Apostolou D, Xydis G. A literature review on hydrogen refuelling stations and infrastructure. Current status and future prospects. Renew Sustain Energy Rev 2019;113:109292.
[17] Low JM, Haszeldine RS, Mouli-Castillo J. Refuelling infrastructure requirements for renewable hydrogen road fuel through the energy transition. Energy Policy 2023;172:113300.
[18] BMWi. Die Nationale Wasserstoffstrategie. Berlin; 2020.
[19] European Commission. In focus: Renewable hydrogen to decarbonise the EU's energy system. [November 17, 2022]; Available from: https://ec.europa.eu/info/news/renewable-hydrogen-decarbonise-eus-energy-system-2022-nov-15_en.
[20] Velazquez Abad A, Dodds PE. Green hydrogen characterisation initiatives: definitions, standards, guarantees of origin, and challenges. Energy Policy 2020;138(2):111300.
[21] Biresselioglu ME, Demirbag Kaplan M, Yilmaz BK. Electric mobility in Europe: a comprehensive review of motivators and barriers in decision making processes. Transp Res A Policy Pract 2018;109:1–13.
[22] Browne D, O'Mahony M, Caulfield B. How should barriers to alternative fuels and vehicles be classified and potential policies to promote innovative technologies be evaluated? J Clean Prod 2012;35:140–51.
[23] Astiaso GD. Analysis of non-economic barriers for the deployment of hydrogen technologies and infrastructures in European countries. Int J Hydrogen Energy 2017;42(10):6435–47.
[24] Gustafsson M, Svensson N, Eklund M, Dahl Öberg J, Vehabovic A. Well-to-wheel greenhouse gas emissions of heavy-duty transports: influence of electricity carbon intensity. Transp Res Part D: Transp Environ 2021;93:102757.
[25] Bussar C, Stöcker P, Cai Z, Moraes Jr L, Magnor D, Wiernes P, et al. Large-scale integration of renewable energies and impact on storage demand in a European renewable power system of 2050—sensitivity study. J Storage Mater 2016;6(4):1–10.
[26] Soares J, Almeida J, Gomes L, Canizes B, Vale Z, Neto E. Electric vehicles local flexibility strategies for congestion relief on distribution networks. Energy Rep 2022;8:62–9.
[27] Mansour-Saatloo A, Ebadi R, Mirzaei MA, Zare K, Mohammadi-Ivatloo B, Marzband M, et al. Multi-objective IGDT-based scheduling of low-carbon multi-energy microgrids integrated with hydrogen refueling stations and electric vehicle parking lots. Sustain Cities Soc 2021;74:103197.
[28] Rose PK, Neumann F. Hydrogen refueling station networks for heavy-duty vehicles in future power systems. Transp Res Part D: Transp Environ 2020;83:102358.
[29] Haupt L, Schöpf M, Wederhake L, Weibelzahl M. The influence of electric vehicle charging strategies on the sizing of electrical energy storage systems in charging hub microgrids. Appl Energy 2020;273(1):115231.
[30] Baumgarte F, Glenk G, Rieger A. Business models and profitability of energy storage. iScience 2020;23(10):101554.
[31] Ton DT, Smith MA, The US. Department of energy's microgrid initiative. Electr J 2012;25(8):84–94.
[32] Hirsch A, Parag Y, Guerrero J. Microgrids: a review of technologies, key drivers, and outstanding issues. Renew Sustain Energy Rev 2018;90:402–11.
[33] Sabadini F, Madlener R. The economic potential of grid defection of energy prosumer households in Germany. Adv Appl Energy 2021;4(5):100075.
[34] Mah AXY, Ho WS, Hassim MH, Hashim H, Ling GHT, Ho CS, et al. Optimization of a standalone photovoltaic-based microgrid with electrical and hydrogen loads. Energy 2021;235:121218.
[35] Jacob AS, Banerjee R, Ghosh PC. Sizing of hybrid energy storage system for a PV based microgrid through design space approach. Appl Energy 2018;212:640–53.
[36] Zhao L, Brouwer J. Dynamic operation and feasibility study of a self-sustainable hydrogen fueling station using renewable energy sources. Int J Hydrogen Energy 2015;40(10):3822–37.
[37] Li B, Roche R, Paire D, Miraoui A. Sizing of a stand-alone microgrid considering electric power, cooling/heating, hydrogen loads and hydrogen storage degradation. Appl Energy 2017;205(2):1244–59.
[38] Bahramirad S, Reder W, Khodaei A. Reliability-constrained optimal sizing of energy storage system in a microgrid. IEEE Trans Smart Grid 2012;3(4):2056–62.
[39] Baumgarte F, Kaiser M, Keller R. Policy support measures for widespread expansion of fast charging infrastructure for electric vehicles. Energy Policy 2021;156(7):112372.
[40] Xiang Y, Cai H, Liu J, Zhang X. Techno-economic design of energy systems for airport electrification: a hydrogen-solar-storage integrated microgrid solution. Appl Energy 2021;283:116374.
[41] Ding H, Hu Z, Song Y. Value of the energy storage system in an electric bus fast charging station. Appl Energy 2015;157:630–9.
[42] Khiareddine A, Ben Salah C, Rekioua D, Mimouni MF. Sizing methodology for hybrid photovoltaic /wind/ hydrogen/battery integrated to energy management strategy for pumping system. Energy 2018;153:743–62.
[43] Alam M, Kumar K, Dutta V. Design and analysis of fuel cell and photovoltaic based 110 V DC microgrid using hydrogen energy storage. Energy Storage 2019;1(3):255.
[44] Valverde L, Rosa F, Bordons C. Design, planning and management of a hydrogen-based microgrid. IEEE Trans Ind Inf 2013;9(3):1398–404.
[45] Alavi F, Park Lee E, van de Wouw N, de Schutter B, Lukszo Z. Fuel cell cars in a microgrid for synergies between hydrogen and electricity networks. Appl Energy 2017;192:296–304.
[46] Baghaee HR, Mirsalim M, Gharehpetian GB, Talebi HA. Reliability/cost-based multi-objective Pareto optimal design of stand-alone wind/PV/FC generation microgrid system. Energy 2016;115(1):1022–41.
[47] Vafaei M, Kazerani M. Optimal unit-sizing of a wind-hydrogen-diesel microgrid system for a remote community. IEEE Trondheim PowerTech 2011;2011:1–7.
[48] Xu X, Hu W, Di Cao, Huang Q, Liu W, Jacobson MZ et al. Optimal operational strategy for an offgrid hybrid hydrogen/electricity refueling station powered by solar photovoltaics. J Power Sources 2020;451(46):227810.
[49] Coppitters D, de Paepe W, Contino F. Robust design optimization and stochastic performance analysis of a grid-connected photovoltaic system with battery storage and hydrogen storage. Energy 2020;213:118798.
[50] Tobajas J, Garcia-Torres F, Roncero-Sánchez P, Vázquez J, Bellatreche L, Nieto E. Resilience-oriented schedule of microgrids with hybrid energy storage system using model predictive control. Appl Energy 2022;306:118092.
[51] Yamashita DY, Vechiu I, Gaubert J-P. Two-level hierarchical model predictive control with an optimised cost function for energy management in building microgrids. Appl Energy 2021;285:116420.
[52] Aslani M, Imanloozadeh A, Hashemi-Dezaki H, Hejazi MA, Nazififard M, Ketabi A. Optimal probabilistic reliability-oriented planning of islanded microgrids considering hydrogen-based storage systems, hydrogen vehicles, and electric vehicles under various climatic conditions. J Power Sources 2022;525:231100.
[53] Kyriakarakos G, Dounis AI, Rozakis S, Arvanitis KG, Papadakis G. Polygeneration microgrids: a viable solution in remote areas for supplying power, potable water and hydrogen as transportation fuel. Appl Energy 2011;88(12):4517–26.
[54] Grüger F, Dylewski L, Robinius M, Stolten D. Carsharing with fuel cell vehicles: Sizing hydrogen refueling stations based on refueling behavior. Appl Energy 2018;228:1540–9.
[55] Xu Y-P, Liu R-H, Tang L-Y, Wu H, She C. Risk-averse multi-objective optimization of multi-energy microgrids integrated with power-to-hydrogen technology,

electric vehicles and data center under a hybrid robust-stochastic technique. Sustain Cities Soc 2022;79:103699.
[56] Han Y, Zhang G, Li Q, You Z, Chen W, Liu H. Hierarchical energy management for PV/hydrogen/battery island DC microgrid. Int J Hydrogen Energy 2019;44(11):5507–16.
[57] Han Y, Yang H, Li Q, Chen W, Zare F, Guerrero JM. Mode-triggered droop method for the decentralized energy management of an islanded hybrid PV/hydrogen/battery DC microgrid. Energy 2020;199:117441.
[58] Dawood F, Shafiullah GM, Anda M. Stand-alone microgrid with 100% renewable energy: a case study with hybrid solar PV-battery-hydrogen. Sustainability 2020;12(5):2047.
[59] Dispenza G, Sergi F, Napoli G, Randazzo N, Di Novo S, Micari S, et al. Development of a solar powered hydrogen fueling station in smart cities applications. Int J Hydrogen Energy 2017;42(46):27884–93.
[60] Liu J, Cao S, Chen X, Yang H, Peng J. Energy planning of renewable applications in high-rise residential buildings integrating battery and hydrogen vehicle storage. Appl Energy 2021;281:116038.
[61] Vivas FJ, Segura F, Andújar JM, Caparrós JJ. A suitable state-space model for renewable source-based microgrids with hydrogen as backup for the design of energy management systems. Energ Conver Manage 2020;219(1):113053.
[62] Zhang X, Pei W, Mei C, Deng W, Tan J, Zhang Q. Transform from gasoline stations to electric-hydrogen hybrid refueling stations: an islanding DC microgrid with electric-hydrogen hybrid energy storage system and its control strategy. Int J Electr Power Energy Syst 2022;136:107684.
[63] Perea E, Oyarzabal JM, Rodríguez R. Definition, evolution, applications and barriers for deployment of microgrids in the energy sector. Elektrotech Inftech 2008;125(12):432–7.
[64] Elsayed AT, Mohamed AA, Mohammed OA. DC microgrids and distribution systems: an overview. Electr Pow Syst Res 2015;119(May–June):407–17.
[65] Lotfi H, Khodaei A. AC versus DC microgrid planning. IEEE Trans Smart Grid 2017;8(1):296–304.
[66] Ullah S, Haidar AMA, Zen H. Assessment of technical and financial benefits of AC and DC microgrids based on solar photovoltaic. Electr Eng 2020;102(3):1297–310.
[67] Tabari M, Yazdani A. A DC distribution system for power system integration of plug-in hybrid electric vehicles. IEEE Power Energy Soc Gen Meet 2013:1–5.
[68] Noriega BE, Pinto RT, Bauer P. Sustainable DC-microgrid control system for electric-vehicle charging stations. In: 15th European conference on power electronics and applications (EPE); 2013. p. 1–10.
[69] Megía PJ, Vizcaíno AJ, Calles JA, Carrero A. Hydrogen production technologies: from fossil fuels toward renewable sources. A mini review. Energy Fuels 2021;35(20):16403–15.
[70] Grigoriev SA, Fateev VN, Bessarabov DG, Millet P. Current status, research trends, and challenges in water electrolysis science and technology. Int J Hydrogen Energy 2020;45(49):26036–58.
[71] Hassan IA, Ramadan HS, Saleh MA, Hissel D. Hydrogen storage technologies for stationary and mobile applications: review, analysis and perspectives. Renew Sustain Energy Rev 2021;149(3):111311.
[72] Acar C, Dincer I. Impact assessment and efficiency evaluation of hydrogen production methods. Int J Energy Res 2015;39(13):1757–68.
[73] Nitta N, Wu F, Lee JT, Yushin G. Li-ion battery materials: present and future. Mater Today 2015;18(5):252–64.
[74] Töpler J, Lehmann J. Wasserstoff und Brennstoffzelle. Berlin, Heidelberg: Springer, Berlin Heidelberg; 2017.
[75] Cigolotti V, Genovese M, Fragiacomo P. Comprehensive review on fuel cell technology for stationary applications as sustainable and efficient poly-generation energy systems. Energies 2021;14(16):4963.
[76] Jiao K, Xuan J, Du Q, Bao Z, Xie B, Wang B, et al. Designing the next generation of proton-exchange membrane fuel cells. Nature 2021;595(7867):361–9.
[77] Mahmoud MS, Saif Ur Rahman M, A.L.-Sunni FM. Review of microgrid architectures – a system of systems perspective. IET Renew Power Generat 2015;9(8):1064–78.
[78] Alzahrani A, Ferdowsi M, Shamsi P, Dagli CH. Modeling and simulation of microgrid. Proc Comput Sci 2017;114:392–400.
[79] Jamshidi M. System of systems engineering - new challenges for the 21st century. IEEE Aerosp Electron Syst Mag 2008;23(5):4–19.
[80] Su W, Wang J. Energy management systems in microgrid operations. Electr J 2012;25(8):45–60.
[81] Dawoud SM, Lin X, Okba MI. Hybrid renewable microgrid optimization techniques: a review. Renew Sustain Energy Rev 2018;82:2039–52.
[82] Riffonneau Y, Bacha S, Barruel F, Ploix S. Optimal power flow management for grid connected PV systems with batteries. IEEE Trans Sustain Energy 2011;2(3):309–20.
[83] Skoplaki E, Palyvos JA. On the temperature dependence of photovoltaic module electrical performance: a review of efficiency/power correlations. Sol Energy 2009;83(5):614–24.
[84] Luque A, Hegedus S. Handbook of photovoltaic science and engineering. Chichester, UK: John Wiley & Sons, Ltd; 2003.
[85] Birkl CR, Roberts MR, McTurk E, Bruce PG, Howey DA. Degradation diagnostics for lithium ion cells. J Power Sources 2017;341(1):373–86.
[86] Olivier P, Bourasseau C, Bouamama B. Dynamic and multiphysic PEM electrolysis system modelling: a bond graph approach. Int J Hydrogen Energy 2017;42(22):14872–904.
[87] Mench MM. Fuel cell engines. Hoboken, NJ: Wiley; 2008.
[88] Lauf T, Memmler M, Schneider S. Emissionsbilanz erneuerbarer Energieträger: Bestimmung der vermiedenen Emissionen im Jahr 2020. Dessau-Roßlau; 2021.
[89] European Commission. Trans-European Transport Network (TEN-T). [November 17, 2022]; Available from: https://transport.ec.europa.eu/transport-themes/infrastructure-and-investment/trans-european-transport-network-ten-t_en.
[90] BASt. Automatische Straßenverkehrszählung: Data obtained for 2019, 2020 and 2021 at the counting station 9013 in Zusmarshausen, Germany. [November 17, 2022]; Available from: https://www.bast.de/DE/Verkehrstechnik/Fachthemen/v2-verkehrszaehlung/zaehl_node.html.
[91] KBA. Der Fahrzeugbestand im Überblick am 1. Januar 2019 gegenüber dem 1. Januar 2018. [November 17, 2022]; Available from: https://www.kba.de/DE/Statistik/Fahrzeuge/Bestand/Jahrebilanz_Bestand/2019/2019_b_ueberblick_pdf.
[92] KBA. Der Fahrzeugbestand im Überblick am 1. Januar 2020 gegenüber dem 1. Januar 2019. [November 17, 2022]; Available from: https://www.kba.de/DE/Statistik/Fahrzeuge/Bestand/Jahrebilanz_Bestand/2020/2020_b_ueberblick_pdf.
[93] KBA. Der Fahrzeugbestand im Überblick am 1. Januar 2021 gegenüber dem 1. Januar 2020. [November 17, 2022]; Available from: https://www.kba.de/DE/Statistik/Fahrzeuge/Bestand/Jahrebilanz_Bestand/2021/2021_b_ueberblick_pdf.
[94] aleo solar AG. Solarmodul aleo P23L330. [November 17, 2022]; Available from: https://www.aleo-solar.com/app/uploads/sites/2/2016/02/P23_320-330W_DE_web.pdf.
[95] Solcast. Historical Solar Irradiance Data for Location Zusmarshausen, Germany 01.01.2019 - 31.12.2019 and 01.01.2020 - 31.12.2020. [December 27, 2021]; Available from: https://solcast.com/.
[96] ENTSO-E. Day-ahead Prices: Data related to the years 2019, 2020 and 2021 for the German Luxembourg bidding zone; Available from: https://transparency.entsoe.eu/transmission-domain/r2/dayAheadPrices/show.
[97] LEW. Entgelte für Netznutzung Jahresleistungspreissystem. [November 17, 2022]; Available from: https://www.lew-verteilnetz.de/media/1181/j-w-n-db-dvd-internet_intranet-internet-internet-ab-07-2016-netztentgelte-preisblaetter-2019-entgueltig-preisblatt_1-10_2019_e.pdf.
[98] ENTSO-E. Actual Generation per Production Type: Data related to the years 2019, 2020 and 2021 for the German Luxembourg bidding zone. [November 17, 2022]; Available from: https://transparency.entsoe.eu/generation/r2/actualGenerationPerProductionType/show.
[99] LEW. Entgelte für Netznutzung Jahresleistungspreissystem. [November 17, 2022]; Available from: https://www.lew-verteilnetz.de/media/2052/netzentgelte_gesamt_pb1-10a_0107-31122020.pdf.
[100] LEW. Entgelte für Netznutzung Jahresleistungspreissystem. [October 29, 2022]; Available from: https://www.lew-verteilnetz.de/media/2256/preisblaetter_netzentgelte_1-10a_2021.pdf.
[101] Umweltbundesamt. Vergleich der durchschnittlichen Emissionen einzelner Verkehrsmittel im Personenverkehr in Deutschland. [December 12, 2022]; Available from: https://www.umweltbundesamt.de/sites/default/files/medien/366/bilder/dateien/uba_emissionstabelle_personenverkehr_2020.pdf.
[102] Umweltbundesamt. Vergleich der durchschnittlichen Emissionen einzelner Verkehrsmittel im Güterverkehr in Deutschland. [December 12, 2022]; Available from: https://www.umweltbundesamt.de/sites/default/files/medien/366/bilder/dateien/uba_emissionstabelle_gueterverkehr_2020.pdf.
[103] Weiss M, Cloos KC, Helmers E. Energy efficiency trade-offs in small to large electric vehicles. Environ Sci Eur 2020;32(1).
[104] Schäfer P. Daimler zeigt Brennstoffzellen-Lkw Mercedes-Benz GenH2 Truck; 2020.
[105] Hesse H, Schimpe M, Kucevic D, Jossen A. Lithium-ion battery storage for the grid—a review of stationary battery storage system design tailored for applications in modern power grids. Energies 2017;10(12):2107.
[106] Wang S, Lu L, Han X, Ouyang M, Feng X. Virtual-battery based droop control and energy storage system size optimization of a DC microgrid for electric vehicle fast charging station. Appl Energy 2020;259:114146.
[107] Chandra Mouli GR. Charging electric vehicles from solar energy: power converter, charging algorithm and system design; 2018.
[108] Sterner M, Stadler I. Energiespeicher - Bedarf, Technologien, Integration. Berlin, Heidelberg: Springer, Berlin Heidelberg; 2014.
[109] Ballard Power Systems. Product Specifications FC wave. [November 17, 2022]; Available from: https://www.ballard.com/docs/default-source/spec-sheets/fcwavetm-specification-sheet.pdf?sfvrsn=6e44dd80_8.
[110] H-TEC SYSTEMS. H-TEC PEM Electrolyser ME450/1400: Technical system parameters ME450/1400. [November 17, 2022]; Available from: https://www.h-tec.com/en/products/detail/h-tec-pem-electrolyser-me450-1400/me450-1400/.
[111] Kroniger D, Madlener R. Hydrogen storage for wind parks: a real options evaluation for an optimal investment in more flexibility. Appl Energy 2014;136:931–46.
[112] Ueckerdt F, Bauer C, Dirnaichner A, Everall J, Sacchi R, Luderer G. Potential and risks of hydrogen-based e-fuels in climate change mitigation. Nat Clim Chang 2021;11(5):384–93.
[113] Sensfuß F, Ragwitz M, Genoese M. The merit-order effect: a detailed analysis of the price effect of renewable electricity generation on spot market prices in Germany. Energy Policy 2008;36(8):3086–94.